

# To Bin or Not To Bin: Decorrelating the Cosmic Equation of State

Roland de Putter & Eric V. Linder  
*Berkeley Lab & University of California, Berkeley, CA 94720*  
(Dated: October 29, 2018)

The physics behind the acceleration of the cosmic expansion can be elucidated through comparison of the predictions of dark energy equations of state to observational data. In seeking to optimize this, we investigate the advantages and disadvantages of using principal component analysis, uncorrelated bandpowers, and the equation of state within redshift bins. We demonstrate that no one technique is a panacea, with tension between clear physical interpretation from localization and from decorrelated errors, as well as model dependence and form dependence. Specific lessons include the critical role of proper treatment of the high redshift expansion history and the lack of a unique, well defined signal-to-noise or figure of merit.

## I. INTRODUCTION

The acceleration of the universe poses a fundamental mystery to cosmology, gravitation, and quantum physics. Understanding the nature of the dark energy responsible for the acceleration relies on careful, robust measurements of the dark energy properties, in particular its equation of state (EOS), or pressure to energy density, ratio that directly enters the Friedmann equation for cosmic acceleration. As scientists design the next generation of dark energy experiments they seek to optimize the measurements for the clearest insight into this unknown physics.

Two critical pieces of information will be the value of the EOS at some epoch, such as the present, and a measure of its time variation, in much the way that early universe inflation theories are classified by the value of the spectral index and its running. The best parametrized EOS are physics based and model independent, i.e. able to describe dark energy dynamics globally, or at least over a wide range of behaviors. Such EOS are very successful at fitting to data and projecting the results of future experiments, and can be robust to bias against inexact parametrization.

Other approaches seek to remove one drawback of parametrized EOS by not assuming a functional form for the time variation, lest the true dark energy model lie outside the apparently wide range of validity of the form, i.e. they aim for form independence. Two major avenues for achieving this are decomposition into basis functions or principal components (e.g. [1], also see [2, 3, 4, 5, 6, 7]) and individual values of the EOS  $w(z)$  over finite redshift bins, which become more general as the number of elements increases. However uncertainties in estimation of the EOS properties also grow as the number of principal components or bins increases.

This article begins by examining general properties of the cosmological data and its dependence on the EOS in §II. Many of the later, detailed results will already be foreshadowed by this straightforward and general analysis. In §III we examine principal component analysis of the EOS and in §IV uncorrelated bandpowers. Bins of EOS in redshift is investigated in §V, including figures of merit for quantifying the uncertainties. Further concentration on the crucial role of the high redshift EOS, and the risk of biasing parameter estimation, occurs in §VI. We consider physical constraints on EOS properties in §VII and summarize our results and conclude in §VIII.

## II. COSMOLOGICAL INFORMATION AND THE EQUATION OF STATE

Cosmological observations probe the EOS through its influence on the cosmic expansion history and the growth history of massive structures. The relation involves in general an integral (or double integral) over the EOS. This implies that the kernel, or response of the observables to the EOS, is broad in redshift, not tightly localized. For distances, the EOS at one redshift formally influences distances at all higher redshifts, while for growth variables that EOS value influences all lower redshifts; this implies a certain skewness. After setting up the simulated observations, we demonstrate that cosmological information is difficult to simultaneously localize and decorrelate, as well as highlighting some necessary cautions regarding treatment of data and priors.

## A. Cosmological Variables

Information inherent in measurements of cosmological quantities regarding the EOS and other parameters can be estimated through the Fisher information matrix,

$$F_{ij} = \sum_{k,k'} \frac{\partial O_k}{\partial p_i} COV^{-1}[O_k, O_{k'}] \frac{\partial O_{k'}}{\partial p_j}, \quad (1)$$

where  $\partial O_k/\partial p_i$  gives the sensitivity of observable  $O_k$  to parameter  $p_i$ , and  $COV$  gives the measurement covariance matrix. One often takes the measurement errors to be diagonal,  $COV \rightarrow \sigma_k^2 \delta_{kk'}$ . Alternately one could use another likelihood estimator such as a Monte Carlo Markov Chain; the general results will not change. Each observable depends on the EOS and other parameters such as the present matter density relative to the critical density,  $\Omega_m$ .

For the EOS, we begin by dividing the redshift interval  $(0, z_{\max})$  into  $N$  bins of not necessarily equal widths  $\Delta z_i$  ( $i = 1, \dots, N$ ), where  $\sum_i \Delta z_i = z_{\max}$ . The index  $i$  is taken to increase with  $z$ . The equation of state is written as

$$w(z) - w_b(z) = \alpha_i e_i(z) \quad (2)$$

(repeated indices are to be summed over), where  $e_i(z) = 1$  inside the  $i$ th bin and zero outside. Such a binning is general, and serves as the first step for investigation of principal components (§III), decorrelated bandpowers (§IV), or straight binning (§V).

The  $N$  coefficients  $\alpha_i$  are the parameters describing the EOS in this model. Note that these coefficients measure the equation of state relative to some “baseline” equation of state  $w_b(z)$ . We can choose  $w_b$  to be some model, like the cosmological constant  $\Lambda$  ( $w_b = -1$ ), to which we want to compare the data. We address issues of the baseline EOS and binning variable in §III. For convenience we sometimes write  $e_i(z)$  as  $\mathbf{e}_i$ , and  $\alpha_i$ , in the case where  $\mathbf{e}_i$  is a unit box function, as  $w_i$ .

For cosmological observables, we focus here on various distances, including as measured by Type Ia supernovae (SN), by the cosmic microwave background (CMB) acoustic peaks, and by baryon acoustic oscillation (BAO) patterns in large scale structure. For all these the EOS enters through the Hubble parameter

$$H(z)/H_0 = [\Omega_m (1+z)^3 + \Omega_{DE} f(z)]^{1/2}, \quad (3)$$

where the present dark energy density  $\Omega_{DE} = 1 - \Omega_m$  for a spatially flat universe as assumed here. The function  $f(z)$  is the ratio of the dark energy density at redshift  $z$  to its current energy density. When  $z$  lies in the  $j$ th EOS bin,

$$f(z) = \left( \frac{1+z}{1+z_j} \right)^{3(1+w_j)} \prod_{i=1}^{j-1} \left( \frac{1+z_{i+1}}{1+z_i} \right)^{3(1+w_i)}, \quad (4)$$

where  $z_i$  is the lower redshift bound of the  $i$ th bin (note  $z_1 = 0$ ) and  $w_i$  the fiducial value of the EOS in that bin.

The SN luminosity distance data set extends from redshift zero to  $z_{\max} = 1.7$ , with a distribution and systematic errors as given for the future SNAP mission in [8]. CMB data is treated as a 0.7% constraint on the reduced distance to last scattering,  $d_{\text{ISS}} = (\Omega_m h^2)^{1/2} \int_0^{1089} dz/H(z)$ , as should be available from the Planck mission. In addition to the  $N$  EOS bins between  $z = 0 - z_{\max}$ , we define a single bin for redshifts  $z > z_{\max}$  having averaged, hence constant, EOS  $w_{N+1}$ . Note that freely marginalizing over  $w_{N+1}$  when only one data point depends on this parameter is equivalent to not including the parameter and the data point. We consider BAO in §VI. Thus the Fisher matrix has dimensions  $(N+3) \times (N+3)$ , with  $\Omega_m$  (or equivalently  $\Omega_{DE}$ ) and the parameter  $\mathcal{M}$  giving the combination of SN absolute magnitude and Hubble constant in addition to the  $N+1$  EOS values  $w_i$ . Unless otherwise stated, results shown marginalize over  $\Omega_m$  and  $\mathcal{M}$ .

## B. Information Localization

Ideally, binned EOS would reflect an invariant measure of the information (or conversely, uncertainty) at its particular redshift. Such a mapping between information and local variables, or bandpowers, works well for large scale structure (LSS), even into nonlinear scales, and we follow the approach of [9] but apply it to the EOS. To refine the localization of information one can attempt to use a large number of bins. We initially consider  $N = 100$  EOS bins equally spaced in redshift.

Figure 1 plots five rows of the Fisher information matrix as a representation of the information as a function of redshift. An element  $F(z, z')$  denotes the Fisher matrix entry  $F_{ij}$  with respect to parameters  $p_i = w(z_i = z)$  and

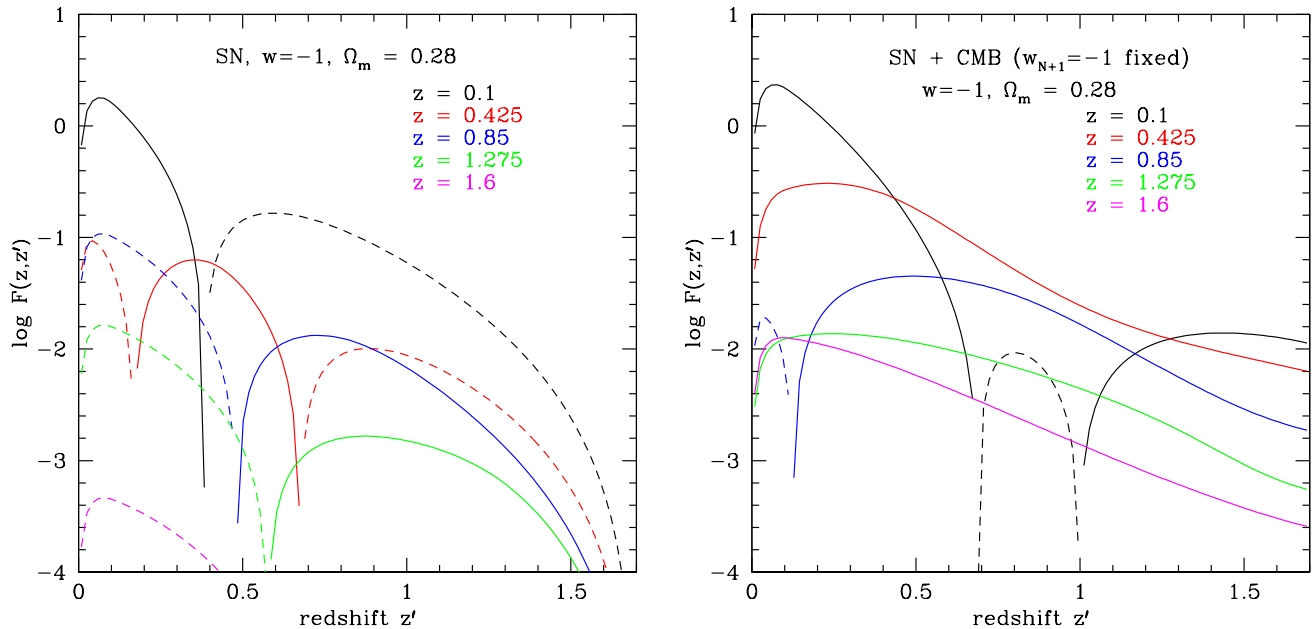


FIG. 1: Five rows (or columns,  $\mathbf{F}$  is symmetric) of the Fisher matrix calculated using a uniform binning in redshift  $z$  ( $N = 100$  bins), showing the cosmological information as a function of redshift. Dashed lines show where  $F_{ij}$  is negative. The first panel uses only supernova data, the second panel includes the distance to CMB last scattering  $d_{\text{ISS}}$ , with the equation of state for  $z = 1.7 - 1089$  fixed to the fiducial value  $w_{N+1} = -1$ . The curves of information are far from sharp spikes at  $z = z'$ , indicating the cosmological information is difficult to localize and decorrelate.

$p_j = w(z_j = z')$ . Note that in contrast to the LSS case (see, e.g., Fig. 1 of [9]), the information is far from localized (the peaks are broad), is not “faithful” (the peaks do not generally peak at  $z = z'$ , especially for large  $z$ ), and is skew (the matrix rows are not symmetric about the peaks). In the LSS case, the peaks were sharp and on the matrix diagonal, with amplitudes some two order of magnitude above the broader “continuum”. For the EOS case the kernels are broad without well defined peaks, and the above properties indicate the matrix is far from diagonal.

Further difficulties arise with respect to localization or characterization of information for the EOS case when considering priors or additional data, and changes in binning or variables. Suppose we add CMB data<sup>1</sup>. As shown in the second panel of Fig. 1, this has three effects: it increases the overall amplitude of the Fisher matrix  $\mathbf{F}$ , broadens the peaks of the rows, and shifts the peaks to lower  $z$ , decreasing their “faithfulness” (moving the peaks further away from where they would be in the diagonal case). The first effect is easy to understand. We add information so  $\mathbf{F}$  becomes larger and uncertainties decrease. The second and third effects can be summarized by saying that  $\mathbf{F}$  is made less diagonal. This is understandable too. The CMB information in  $d_{\text{ISS}}$  has about the same dependence on all low  $z$  EOS parameters and thus adds to their correlation. To check this, Fig. 2 shows the resulting Fisher information when an extremely tight prior is put on CMB data, or the matter density  $\Omega_m$  is fixed. Localization and faithfulness are almost completely lost (the EOS part of the Fisher matrix is far from diagonal).

Information within a localized region is also not invariant when considering changes in the number of bins or binning variable. Note that changing the binning variable from redshift  $z$  to scale factor  $a = (1 + z)^{-1}$  or e-fold factor  $\ln a$  is equivalent to changing the bins to non-uniform widths in  $z$ . Figure 3 demonstrates the variations that occur in the standard deviation of the EOS parameters when considering a binning uniform in  $z$  vs. one uniform in  $a$ , as well as when changing the number of bins  $N$ . A key point is that while the Fisher matrix behaves in a simple fashion when bin spacing is changed (as shown in §III), the uncertainties  $\sigma_i$  – which are square roots of the diagonal elements of the *inverse* of the Fisher matrix – behave in a complicated manner.

<sup>1</sup> We here simultaneously fix the value of the EOS in the one bin beyond the SN data,  $w_{N+1}$ . As mentioned, adding one data point and marginalizing over the one new parameter is equivalent to not including the data and new parameter, i.e. it gives the same Fisher matrix as in the SN only case.

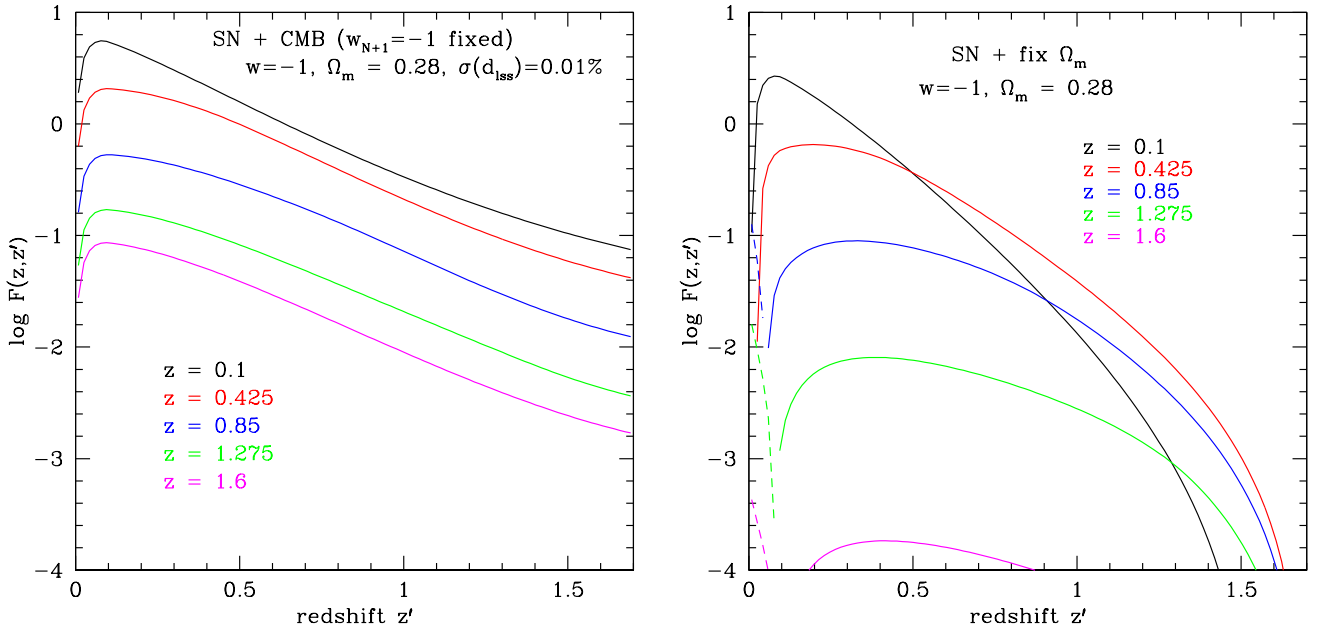


FIG. 2: As Fig. 1, but with a very tight prior on the CMB information  $d_{\text{ISS}}$  (first panel) or fixing the matter density  $\Omega_m$  (second panel).

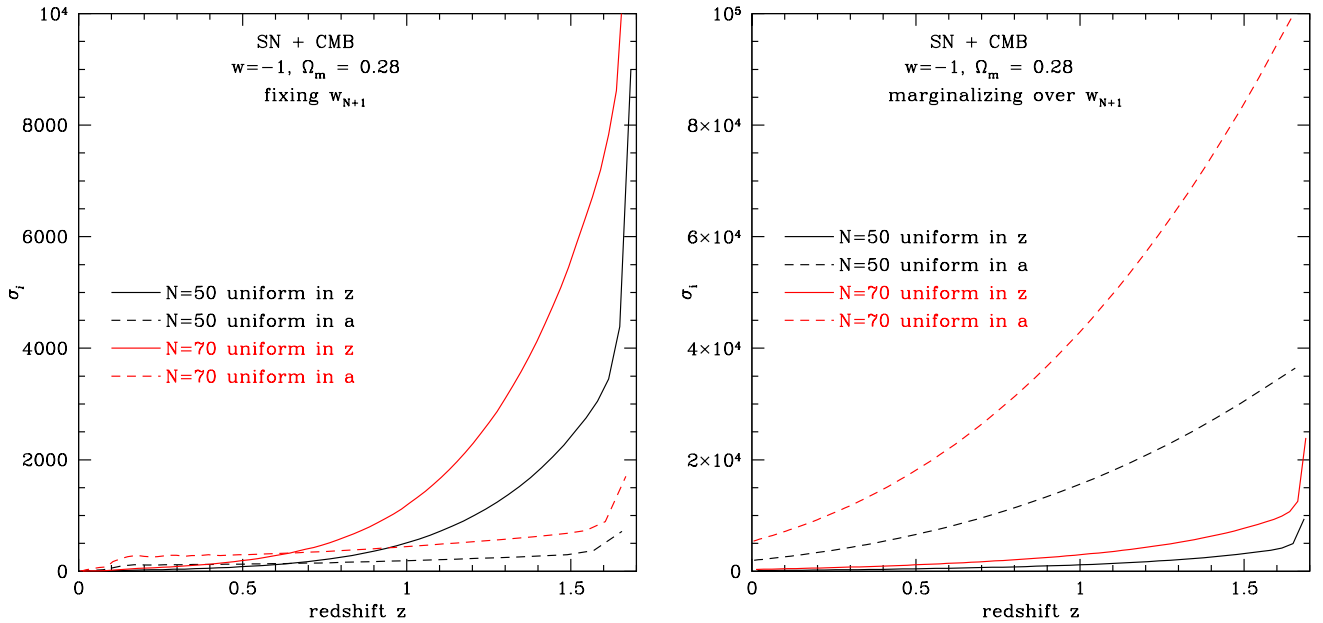


FIG. 3: The standard deviation of the EOS in each bin for 50 and 70 bins uniformly spaced in redshift  $z$  or scale factor  $a$ . The first panel shows the case with fixed  $w_{N+1} = -1$  and the second panel has  $w_{N+1}$  marginalized over. Note that the standard deviation depends on binning variable nontrivially and does not scale with number of bins  $N$  (i.e. the inverse of the bin width) as  $N^{1/2}$ .

First of all, when  $N$  is increased from 50 to 70, and so the bin width is correspondingly reduced for a given binning variable, the  $\sigma$ 's do not simply scale by a factor  $\sqrt{70/50}$  as one might have been tempted to think. Recall that  $N$  is the number of parameter bins not data bins. Thus a localized information quantity like  $d\sigma^{-2}/dz$  does not have any real meaning, being dependent on the number of bins and the binning variable. Second, when considering a change in the binning variable, in the case where we marginalize over  $w_{N+1}$  (here equivalent to using only SN data), a binning uniform in  $a$  gives larger  $\sigma$ 's across all redshifts when compared to the binning uniform in  $z$ , even if we use the same total number of bins in both cases. This is counterintuitive since at low redshift the bins uniform in  $a$  are smaller, and at high redshift they are larger than the uniform  $z$  bins so we would expect the EOS uncertainties to be relatively larger, then smaller, respectively. This indeed occurs when we fix  $w_{N+1}$ .

Exploring this behavior, we find that changes in the present dark energy density overwhelm the EOS parameters. For the higher redshift bins of EOS, the Fisher information is only contributed by the relatively few high redshift data points, and there the Fisher sensitivity to  $\Omega_m$  can be more than an order of magnitude greater than to  $w_i$ . Computations show that only when  $\Omega_m$  is fixed or restricted to a degeneracy surface by the CMB  $d_{\text{ISS}}$  constraint does the natural behavior of the EOS bin parameters with changes in binning become manifest. We conclude that changes of binning variables, or equivalently non-uniform bin widths, affect EOS uncertainties in a nontrivial manner, and the treatment of the high redshift EOS needs care as well.

### C. Extracting the Equation of State

The key lesson of this section has been that there is no well-defined measure for localized information on the EOS. Unlike for the LSS power spectrum, the cosmological EOS information has a very broad kernel and the Fisher matrix is far from diagonal. While one can always adopt a basis to transform the Fisher matrix to diagonal form, we will see that this does not help with localization and so the results cannot be interpreted as actual EOS values at a certain redshift. Another issue is the problem of defining a measure of uncertainty in the EOS estimation that does not depend on the specific binning chosen.

This general analysis foreshadows the problem of actually deciding how to quantify measurement of the EOS and any figure of merit to go along with that. In the following sections we investigate three concrete proposals for the meaning behind EOS measurement. One approach is principal component analysis (PCA; see, e.g. [1, 10, 11, 12, 13]), effectively making the number of bins very large, diagonalizing the Fisher matrix and using its eigenvectors as a basis  $e_i(z)$  in Eq. (2). A second approach is uncorrelated bandpowers, using a small number of bins, diagonalizing and scaling the Fisher matrix in an attempt to localize the decorrelated EOS parameters (see, e.g., [14, 15, 16]). Finally, one can exactly localize the EOS parameters using a few bins, at the price of retaining correlations in their uncertainties. Advantages for a method will come from giving robust insight into the physical nature of dark energy.

## III. PRINCIPAL COMPONENTS

It is important to recognize that PCA the way it is normally applied in astrophysics, e.g. to spectra, is very different from the qualities desired in measuring the EOS. In conventional PCA one wants to maximize the variance, essentially the signal, while for the application of PCA to cosmological parameter estimation ([1, 10, 11, 12, 13]) one wants to minimize the variance because it represents the observational uncertainty. In the former case, using a basis of eigenvectors (or eigenmodes) is very useful because it extracts the specific linear combinations of parameters that have the most signal. In the latter case, at least when applied to the dark energy EOS where we want the small variations of data to be revelatory, i.e. arise from very different EOS and so point to the physics, we will see that it is less obvious what the quantitative advantages of PCA are beyond decorrelating the parameter uncertainties. (PCA is still useful in obtaining impressions of sensitivity, i.e. what qualities of the data are best constrained.) For example, for CMB analysis one still prefers to work with quantities having clear physical interpretations rather than principal components, despite the decorrelation [17].

To decorrelate the EOS characteristics, one diagonalizes the Fisher (or inverse covariance) matrix by applying a basis transformation to a basis of eigenmodes. In this new basis  $e'_i$ ,

$$w(z) - w_b(z) = \alpha'_i e'_i(z), \quad (5)$$

such that the uncertainties in the new parameters  $\alpha'_i$  are uncorrelated. It is important to note that in general the basis vectors, or modes, tell us how to interpret the uncertainties in the parameters  $\alpha'_i$  in terms of their effect on the equation of state function  $w(z)$  through

$$e'_i(z) = \frac{\partial w(z)}{\partial \alpha'_i}. \quad (6)$$

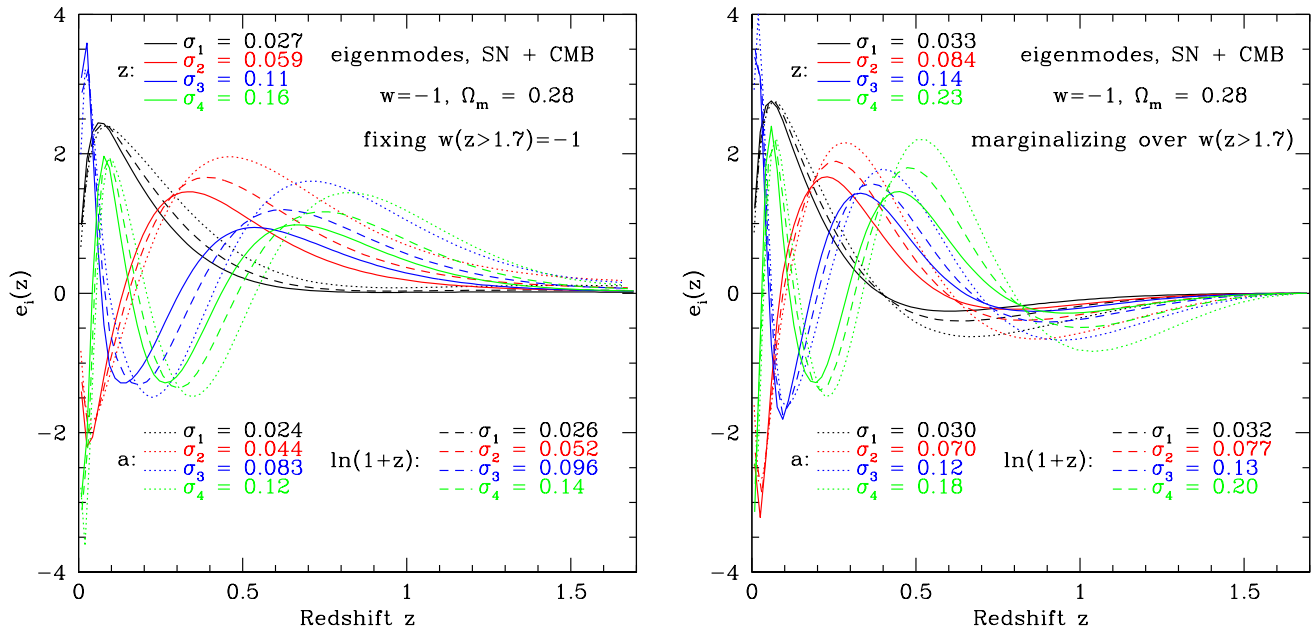


FIG. 4: The first four eigenmodes and their uncertainties calculated using uniform binning in  $z$ ,  $a$  and  $\ln(1+z)$ . In the first panel  $w_{N+1}$  is fixed, in the second panel it is marginalized over. For  $a$  and  $\ln(1+z)$ , the number of EOS bins  $N = 50$ , for  $z$  we use  $N = 100$ , enough for the modes to converge. Note the modes, and their uncertainties, depend on binning variable (even modulo normalization).

We discuss various important mathematical properties regarding modes in Appendix A; here we summarize the most relevant characteristics and results.

- There are an infinite number of bases that decorrelate the coefficients  $\alpha'_i$
- Because the Fisher matrix transforms nontrivially under change of basis, the eigenvectors are not invariant. They are not equivalent between different binning variables or bin widths.
- Each eigenvector has arbitrary normalization and so the meaning of uncertainty in measuring a mode is not well defined.

### A. Eigenmodes

Despite the first point in the list above, we can of course choose a particular basis and work from there. We proceed to do this and illustrate the second and third points. Starting with the unit box basis  $\mathbf{e}_i$  introduced in §II we calculate the eigenmodes (but remember that this set depends on this particular starting point). The fiducial model is  $\Lambda$ CDM:  $w = -1$  with  $\Omega_m = 0.28$  and we consider initial binnings uniform in  $z$ ,  $a$  and  $\ln(1+z)$ .

Figure 4 illustrates the first four modes, after marginalization over  $\Omega_m$  and  $\mathcal{M}$ . For convenience we suppress the primes indicating the new basis. The first panel has the EOS at  $z > 1.7$  fixed to its fiducial value,  $w_{N+1} = -1$ ; in the second panel,  $w_{N+1}$  is treated as a free parameter and marginalized over. For each binning variable or coordinate  $x = z$ ,  $a$ , or  $\ln(1+z)$ , we normalize the modes according to  $\int dx e_i^2(x) = 1$ . Although completely arbitrary, this choice is common.

Note that, as discussed above, the modes (and their respective standard deviations) are different for the different coordinates, even modulo normalization. As the coordinate changes from  $z$  to  $\ln(1+z)$  to  $a$  the modes spread out more, gaining more power at large  $z$  as expected from the relative bin widths. The difference between a binning uniform in a coordinate  $x$  and one uniform in  $z$  depends on the coordinate transformation  $dx/dz$  over the relevant redshift range. Since  $da/dz = -1/(1+z)^2$ ,  $d\ln(1+z)/dz = 1/(1+z)$ , and  $dz/dz = 1$ , this explains the progression.

Also, comparing the modes with  $w_{N+1}$  fixed to those where it is fit from the data shows two things. The uncertainties  $\sigma_i \equiv \sigma(\alpha_i)$  are smaller of course. Second, and perhaps less obvious a priori, the modes are more confined to low redshifts

when  $w_{N+1}$  is made a free parameter. This becomes easier to understand when we remember that marginalizing over  $w_{N+1}$  is equivalent to not using  $d_{\text{ISS}}$  at all. Thus only when  $w_{N+1}$  is fixed does the inclusion of CMB  $d_{\text{ISS}}$  data count, and this spreads the eigenmodes out towards higher  $z$ .

## B. Number of Eigenmodes and their Uncertainties

The eigenmode approach becomes completely general in the limit of an infinite number of bins,  $N \rightarrow \infty$ , as all continuous functions can be constructed from the complete basis. The downside of this is that the uncertainties approach infinity. One compromises by selecting a small set of the best determined modes, i.e. the principal components, and throwing away the others. We face two problems when we try to adopt this approach. The first is the question which set of eigenmodes to begin with (i.e. calculated using which coordinate). The second problem is that “best determined” is not well defined. We elaborate on this below.

As we have demonstrated, calculating the eigenmodes in a different coordinate yields a different set of modes so it is not clear which basis of eigenmodes to choose. Although each *full* basis spans the same space of functions, restricting oneself to the first few eigenmodes with respect to  $z$  gives an essentially different parametrization than using the first few modes with respect to  $a$  or any other coordinate that is not a linear function of  $z$ . The uncertainties will be different and there is the risk that how good one experiment is compared to another will be judged differently.

Even if we have chosen a certain basis, say the eigenmodes arising from uniform binning in the coordinate  $z$ , there is still the issue of quantifying how well determined a mode is. That is, we would like to calculate a measure for how constrained a mode  $\mathbf{e}_i$  is. (Again, we suppress the primes as we will always be interested in the new basis.) An obvious choice seems to be the standard deviation of its coefficient,  $\sigma_i \equiv \sigma(\alpha_i)$ . However, if we rescale  $\mathbf{e}_i$  by a factor  $A$ ,  $\sigma_i$  is rescaled by  $A^{-1}$ . Thus,  $\sigma_i$  only has meaning if we also specify the normalization of the mode, and the normalization is arbitrary, we have no physics guidance in choosing one normalization over another. In fact, it is perfectly legitimate to rescale all modes such that their (coefficients’) uncertainties  $\sigma_i$  are equal to one. Yes, this way it appears many modes have very large fluctuations, but without putting in any physical constraints on  $w(z)$ , i.e. a priori restrictions on the EOS, the word large is meaningless.

Another approach to measuring how well determined a mode is involves using not a pure uncertainty criterion but a signal to noise criterion. This was the approach advocated by [18] but is also problematic. Consider the ratio of the standard deviation  $\sigma_i$  over the coefficient  $\alpha_i$ . At first sight, this seems to solve the problem of normalization as  $\sigma_i/\alpha_i$  is invariant under changes of normalization. However, this approach has its own problems. From the mode expansion

$$w(z) - w_b(z) = \alpha_i e_i(z) \quad (7)$$

we see that the expectation values of the  $\alpha_i$ ’s depend on which baseline function  $w_b(z)$  we expand our measured EOS with respect to. For example, if we use  $w_b = -1$  and the true EOS (or simulated EOS if projecting the leverage of a future survey) is also  $w = -1$ , then the expectation values of the  $\alpha_i$ ’s are all zero. Thus the noise-to-signal  $\sigma_i/\alpha_i$  blows up.

The reason why the quantities  $\sigma_i$  and  $\sigma_i/\alpha_i$  suggested above do not work as measures for how well (or how poorly) determined a mode is, is simple. We have an estimate of the *noise* in the uncorrelated parameters  $\alpha_i$ , but not of the typical *signal* and thus cannot define a proper signal to noise ratio to tell us which modes are well-constrained and which ones are not. It may be tempting to simply throw out modes with large uncertainties, say  $\sigma_i > 1$ , but then we are implicitly making the assumption that the coefficients  $\alpha_i$  are typically of order 1 in the particular normalization – and baseline model – one has chosen for the modes. We have little knowledge on which to base such an assumption.

The method *would* be useful if in addition to knowing the observational uncertainties  $\sigma_i$ , we knew the typical ranges of the  $\alpha_i$ ’s. For example, if we knew the expectation values  $\langle \alpha_i \rangle$  and the typical deviations from their expectation values  $\sqrt{\langle (\alpha_i - \langle \alpha_i \rangle)^2 \rangle}$  (brackets here denote averages over realizations of the parameters, they have nothing to do with observational uncertainties, given by  $\sigma_i$ ), we can call  $\alpha_i$  (and the corresponding mode) well-constrained if the signal to noise ratio

$$\text{SNR} \equiv \frac{\sqrt{\langle (\alpha_i - \langle \alpha_i \rangle)^2 \rangle}}{\sigma_i} \quad (8)$$

is large.

There are two scenarios in which one has knowledge about quantities like  $\langle \alpha_i \rangle$  and  $\sqrt{\langle (\alpha_i - \langle \alpha_i \rangle)^2 \rangle}$ , both quite common in physics. One is when one can observe a (large) sample of realizations of the parameters. If for example the function of interest is a source spectrum (e.g. of quasars or supernovae [19, 20]), the sample size is equal to the number of observed sources. Unfortunately, we can only observe one universe and thus only one equation of state. The other scenario is where one knows what the underlying physics is and what natural values are for the parameters

of the theory (e.g. for the ionization fraction see [13]). For example, if we knew dark energy was described by a scalar field model described by a set of  $n$  parameters and in addition we had a prior probability distribution on those parameters, we could propagate this distribution to the parameters  $\alpha_i$ . Again unfortunately, we have a large number of possible theories for dark energy and little guidance as to the parameter values within those theories. We return to the question of placing physical constraints on the EOS and its modes in §VII.

In conclusion, it is always possible to select a subset of modes and work with those, but it should be realized that what one is doing at that point is putting in assumptions of what the equation of state should look like – precisely what we were trying to avoid by switching to PCA from a functional form – and one cannot call the approach truly form independent anymore.

#### IV. UNCORRELATED BANDPOWERS

While using a large number of bins for the EOS increases the generality of functional forms  $w(z)$ , one ends up with a large number of poorly determined parameters. Instead one could use a small number of bins but perform a basis transformation to decorrelate the parameters. In large scale structure and CMB applications in cosmology this is often called uncorrelated bandpowers, e.g. where the functions are the matter power spectrum binned in wavenumber,  $P(k)$ , or the photon power spectrum binned in multipole,  $C(\ell)$ .

To increase the localization of the modes within the bins, or bands, [9] proposed letting the “square root” of the Fisher matrix define the transformation. See [14] for application specifically to the EOS. Such a transform has the advantage that, in the ideal case, the weights defining the new parameters in terms of the old ones are localized and mostly positive. This would make the new parameters easier to interpret, as true bandpowers, i.e. giving the values of the EOS in a given redshift interval, with uncertainties uncorrelated between bins. Unfortunately we will find that, as presaged in §II, the cosmological EOS analysis is far from the ideal case due to the broadness and skewness of the kernel, in contrast to the LSS case.

##### A. Modes and Weights

We briefly present the procedure for finding the square root of the Fisher matrix and the corresponding transformation. This is placed in the main text because it highlights the important distinction between the properties of the eigenvectors and the weights, which has not always been clear in the literature.

The transformation of interest is given by the symmetric matrix  $\mathbf{W}$  (see Appendix A for our conventions) that transforms the Fisher matrix into the identity matrix:

$$\mathbf{W} \mathbf{F} \mathbf{W}^T = \mathbf{1}. \quad (9)$$

This matrix is constructed using the matrix  $\mathbf{O}$  of which the rows are the (normalized) eigenvectors of  $\mathbf{F}$ , i.e. the orthogonal ( $\mathbf{O}^T = \mathbf{O}^{-1}$ ) matrix that diagonalizes the Fisher matrix

$$\mathbf{O} \mathbf{F} \mathbf{O}^T = \mathbf{D}. \quad (10)$$

$\mathbf{W}$  is now given by

$$\mathbf{W} = \mathbf{O}^T \mathbf{D}^{-1/2} \mathbf{O}, \quad (11)$$

note that the square root of the Fisher matrix  $\mathbf{F}^{1/2} \equiv \mathbf{W}^{-1}$  is also symmetric and it squares to the Fisher matrix (hence the name).

The new basis vectors  $\mathbf{e}'_i$  are now given by the rows of  $\mathbf{W}$  (see Appendix A) and their coefficients  $\alpha'_i$  are

$$\alpha'_i = W_{ji}^{-1} \alpha_j. \quad (12)$$

We follow [14] and rescale the basis vectors and thus  $\mathbf{W}$  such that the  $\alpha'_i$  are weighted averages of the  $\alpha_i$ , i.e. we rescale the rows of  $\mathbf{W}$  such that

$$\sum_{j=1}^N W_{ji}^{-1} = 1. \quad (13)$$



For notational convenience we use the same name for the rescaled transformation matrix  $\mathbf{W}$  as for the original one, but note that after the rescaling  $\mathbf{W}$  is no longer symmetric. The  $\alpha'_i$  are now uncorrelated and their uncertainties are given by

$$\sigma'_i = \left( \sum_{j=1}^N F_{ji}^{1/2} \right)^{-1}. \quad (14)$$

In summary, the rows of  $\mathbf{W}$  contain the new basis vectors  $e'_i$  and the rows of  $(\mathbf{W}^{-1})^T$  contain the weights.

An important point is that even though the weights tell us how to construct the new parameters out of the old ones, as discussed in §III, to interpret the meaning of the uncertainties  $\sigma'_i$  for the EOS one needs to look at the basis vectors  $e'_i(z) = \partial w(z)/\partial \alpha'_i$  and not at the weights. That is,

$$\sigma^2[w(z)] = \sum_i \sigma_i'^2 e_i'^2(z). \quad (15)$$

We emphasize that plots of the weights alone cannot be directly interpreted as values of the EOS. To some extent this confusion has been exacerbated by sometimes writing the weights as  $\mathcal{W}_i$  – these are *not* the EOS  $w_i$ . The distinction between vectors and weights exists because the uncorrelated bandpowers correspond to a non-orthogonal transformation (the only orthogonal transformation decorrelating the parameters is the one to a basis of eigenvectors, as already considered). This distinction will be important to the question of localization and physical interpretation of the parameters. As illustrated in the next section, one can have weights that are all positive while the corresponding basis vectors have significant negative contributions, clouding the interpretation.

### B. Decorrelated Estimates of the Equation of State

Since the matrix of weights is defined as the square root of the Fisher matrix (up to a rescaling to make the weights sum to one), the positivity and localization of the weights depends on how positive and localized the Fisher matrix itself is. The idea of the square root scaling is that the square root is typically narrower, so the weights gain some localization relative to the Fisher matrix. However, we saw in §II that even next generation data probing the EOS involves a very nondiagonal Fisher matrix. This is inherent to the cosmological properties and degeneracies and does not arise from any particular binning or parametrization.

We now calculate the modes described in the previous section. To facilitate comparison to the literature, specifically [14], we choose four low redshift bins with the following ranges:  $z = 0-0.2$ ,  $z = 0.2-0.4$ ,  $z = 0.4-0.6$  and  $z = 0.6-1.7$ . The bins define four EOS parameters  $w_1$  to  $w_4$ . The other cosmological parameters, fiducial values, and data sets are as before. The Fisher matrix for the low  $z$  EOS parameters in the case where  $w_5 \equiv w(z > 1.7)$  is fixed is given by

$$\mathbf{F}_{\text{fix5}} = \begin{pmatrix} 205 & 84 & 17 & 5.8 \\ 84 & 65 & 27 & 19 \\ 17 & 27 & 21 & 21 \\ 5.8 & 19 & 21 & 35 \end{pmatrix} \quad (16)$$

and when  $w_5$  is marginalized over,

$$\mathbf{F}_{\text{marg5}} = \begin{pmatrix} 146 & 33 & -14 & -33 \\ 33 & 22 & 0.66 & -13 \\ -14 & 0.66 & 4.4 & 0.93 \\ -33 & -13 & 0.93 & 10 \end{pmatrix} \quad (17)$$

It is evident that the Fisher matrix is far from diagonal and furthermore that proper treatment of the high redshift EOS behavior, rather than assuming a fixed value for  $w_{N+1}$  (here  $w_5$ ), has a significant effect. For one thing, marginalizing over  $w_5$  introduces negative entries in the Fisher matrix and we will see this causes some of the weights in the decorrelated basis to be negative.

The main results of this section are illustrated in Figs. 5 and 6, giving the uncorrelated modes and the corresponding weights. First consider Fig. 5 where  $w_{N+1}$  is fixed. Previous results (e.g. [14, 15]) showed weights that were almost always positive and strongly localized, i.e. the weights defining the  $i$ th parameter were predominantly peaked in the  $i$ th bin. This implies that the Fisher matrix of the original parameters, including priors, must have been close to diagonal to begin with in those cases. In Fig. 5 the weights are indeed essentially all positive and substantially

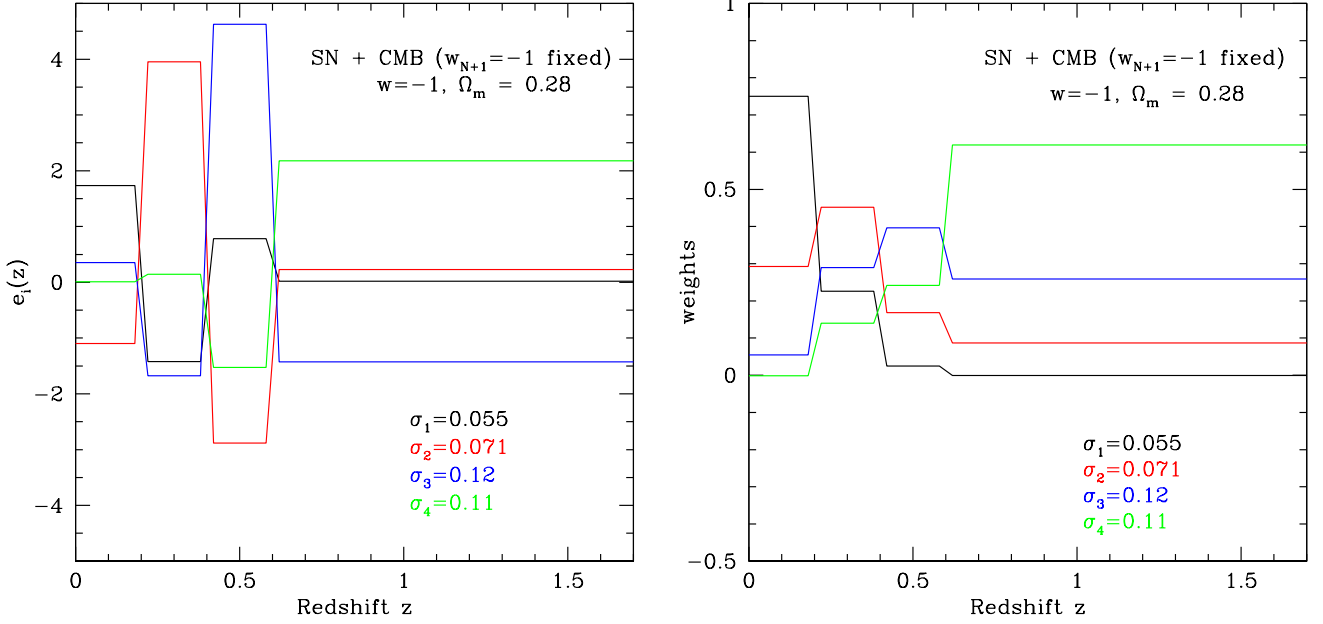


FIG. 5: Uncorrelated basis functions, or modes, (first panel) and weights (second panel) obtained from the square root of the Fisher matrix. Here  $w_5 \equiv w(z > 1.7)$  is fixed to its fiducial value ( $w_5 = -1$ ). Note that the modes have quite different shapes than the plots of the weights; the modes are what gives the impact on EOS  $w(z)$  of an uncertainty  $\sigma_i$ . The weights are only moderately localized (a consequence of the cosmological properties of the original Fisher matrix).

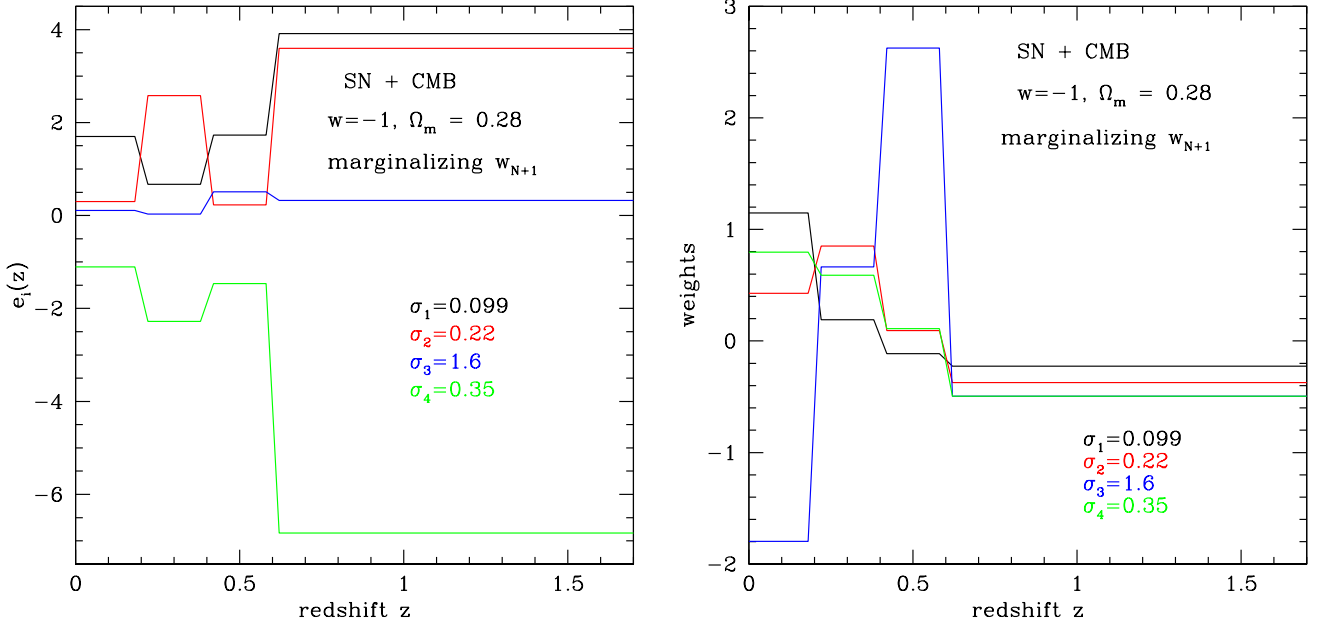


FIG. 6: As Fig. 5, but with  $w_5$  marginalized over. With  $w_5$  as a free parameter, the weights and modes substantially lose their desired properties (being positive and localized).

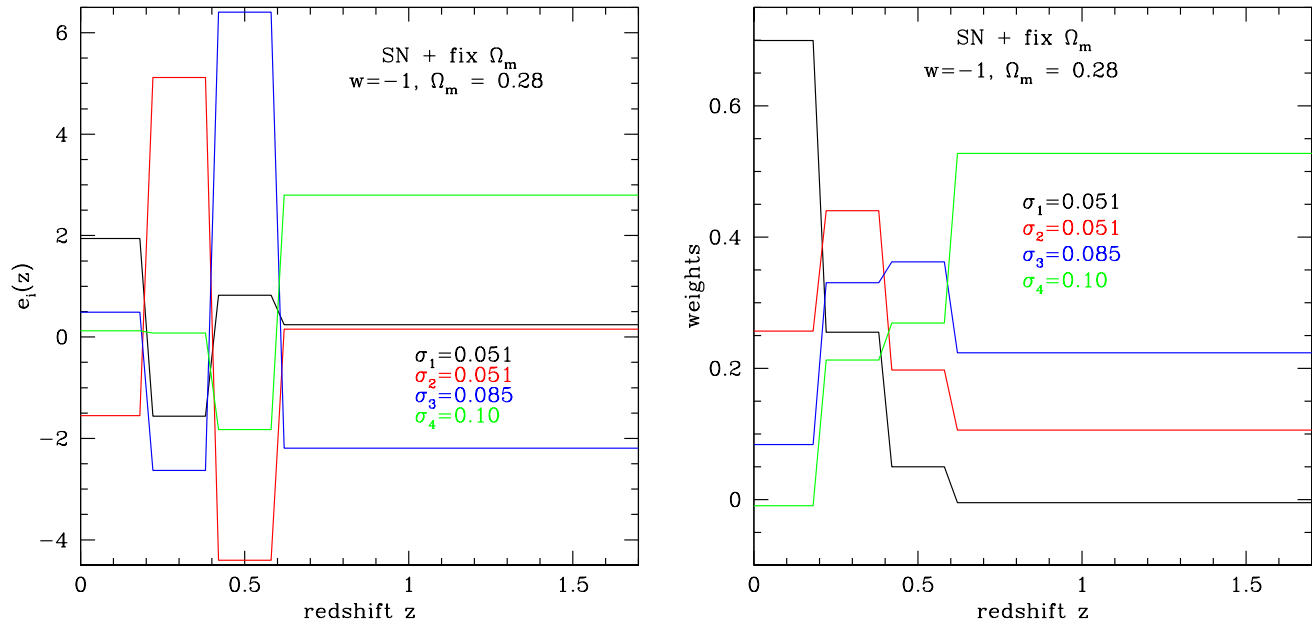


FIG. 7: As Figs. 5 and 6, but instead of using the CMB data point (thus  $w_{N+1}$  does not enter) we fix the matter density  $\Omega_m$ . This illustrates the effect of a tight prior.

localized (slightly less than in the works referred to above but differences in the fiducial model and data could account for this.)

While the characteristics of the weights in the case where  $w_{N+1}$  is fixed look promising, recall that it is the eigenvectors that tell us how to interpret the results in terms of the EOS (see Eqs. 6 and 15). Each (uncorrelated) uncertainty  $\sigma_i = \sigma(\alpha_i)$  derived from the data corresponds to a variation in the EOS behavior  $w(z)$  of the form of the eigenfunction  $e_i(z)$ . We see that the basis functions have quite different shapes than the weights; in particular they have large negative contributions and large oscillations, far from being localized. For example, if  $\alpha_1$  is  $1\sigma$  larger than its fiducial (and the other coefficients are exactly equal to their fiducial values), the EOS in the first bin,  $w_1$ , deviates by  $+1.75 \times 0.055$  from its fiducial value  $-1$ , while the EOS in the second bin,  $w_2$ , deviates almost as strongly but *negatively* by  $-1.45 \times 0.055$  from  $-1$ .

For a deviation in the third coefficient,  $\alpha_3$ , by  $1\sigma$ , the consequences are even more dramatic: a bump in  $w_3$  by  $+4.7 \times 0.12$  and a dip in  $w_2$  by  $-1.7 \times 0.12$ . Note that while the  $\alpha_i$  are decorrelated, the impact on the EOS is not localized, so the values of  $w_i$  remain correlated. Such information is hard to get from just looking at the apparently well-behaved weights (which are often the only quantities plotted).

Much of the good behavior of the weights is an artefact of fixing the high redshift behavior of the EOS, i.e. imposing a form (in a supposedly form independent approach). When we instead allow freedom in  $w_{N+1}$  and marginalize over it, the effects are dramatic as seen in Fig. 6. This is not surprising given the differences in the respective Fisher matrices, Eqs. (16) and (17). Some of the weights now have considerably negative values and the modes are certainly not localized in the expected bin. Instead, all of them have substantial power in the highest redshift bin shown.

To verify that it is the strength of the prior information, and not the square root of the Fisher matrix scaling per se, that causes the weights in Fig. 5 (and the literature examples) to look so well behaved, we imposed ever tighter priors on  $\Omega_m$ . When the prior is weak, the weights are both positive and negative. As the prior tightens, the weights become progressively more positive and localized. Figure 7 shows the limit as we fix  $\Omega_m$ .

### C. Continuum Limit

To ensure that the breakdown in positivity and locality of the weights is not an artefact of the binning, but rather is inherent to the cosmological data probing the EOS, we take the continuum limit,  $N \gg 1$ . Figures 8 and 9 plot the uncorrelated modes and weights corresponding to the square root of the Fisher matrix for  $N = 100$ . We see that even in this limit the modes fluctuate heavily and the weights are not very localized (which makes sense because they

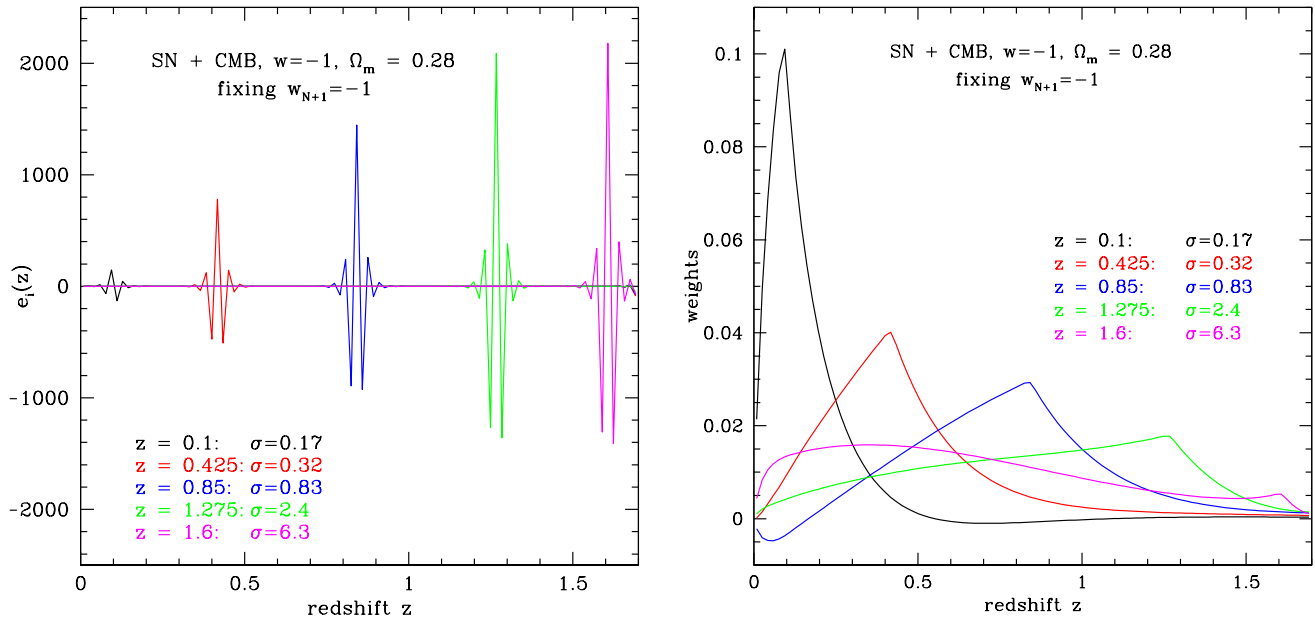


FIG. 8: Illustration of what the modes (first panel) and weights (second panel) based on  $\mathbf{F}^{1/2}$  look like in the large  $N$  case, here  $N = 100$ . Here we fix  $w_{N+1} = -1$ .

are given by the square root of the Fisher matrix depicted in Fig. 1) though they are more faithful, i.e. peak at the given redshift. Again, the physically appropriate act of marginalizing over  $w_{N+1}$  removes most vestiges of the desired positivity and locality.

The conclusion is that to obtain truly localized weights implies that one already started with a substantially localized (peaked, with a narrow kernel) inverse covariance matrix  $\mathbf{F}$ . In such a case the EOS parameters are already easy to interpret without decorrelating them. Conversely, having weights that do not become tightly localized (and we have shown they may not without a strong external prior) implies that the new basis parameters are hard to interpret – one might as well stick to the original correlated parameters. Thus, like PCA, using the square root of the Fisher matrix in an attempt to obtain uncorrelated bandpowers is not a panacea in the quest for understanding dark energy.

## V. BINNED EQUATION OF STATE

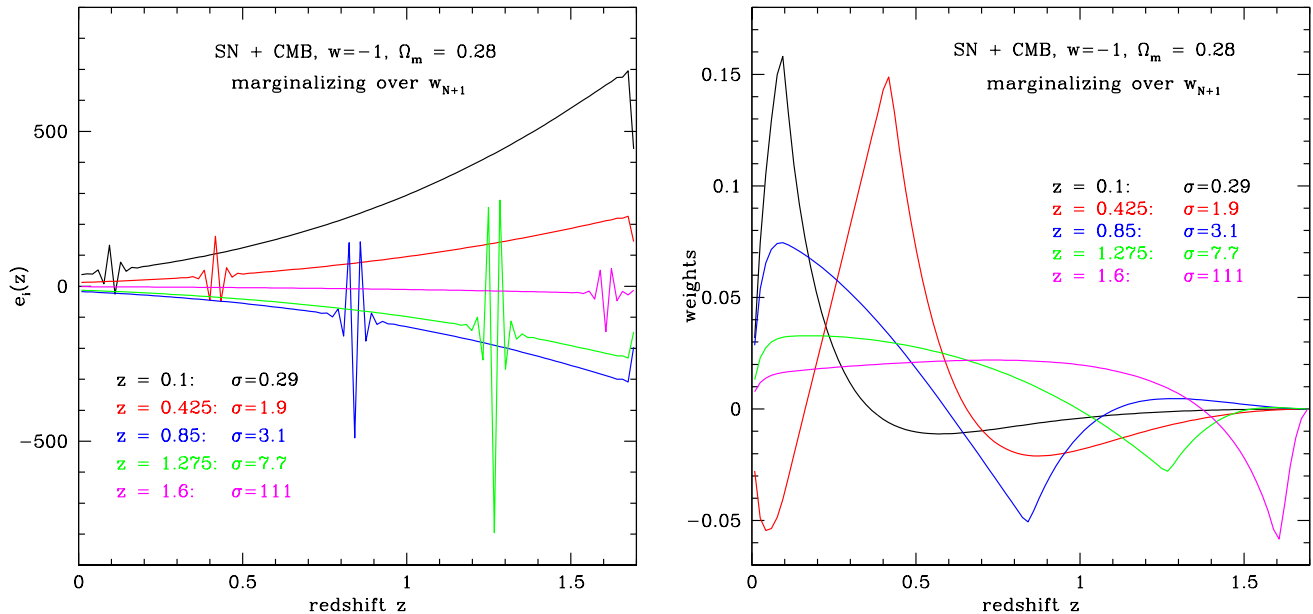
The third approach to understanding the EOS is simply considering the values in a small number of redshift bins. That is, one defines piecewise constant EOS in some redshift range, e.g.  $w(z) = w_i$  when  $z_i < z < z_{i+1}$  (like in §IV, but without decorrelating). This guarantees localization and straightforward physical interpretation, at the price of some correlation in the uncertainties. As we have seen, however, one cannot in practice generally have both localization and no correlation.

### A. Uncertainties and Correlations

Calculation of the EOS estimation is straightforward. Here we concentrate on questions of sensitivity to changes in binning and to treatment of the high redshift bin, rather than specific numbers for the uncertainties. To see the trends most clearly, we consider only two bins below  $z = 1.7$  along with the one at higher redshift.

The quantities of interest are the uncertainties  $\sigma_i$  on the EOS values (marginalizing over the other cosmological parameters), the correlation coefficients between EOS values,

$$r_{ij} = \frac{C_{ij}}{\sigma_i \sigma_j}, \quad (18)$$

FIG. 9: As Fig. 8, but marginalizing over  $w_{N+1}$ .

and the global correlation coefficients [21]

$$r_i = \sqrt{1 - \frac{1}{C_{ii}F_{ii}}}, \quad (19)$$

which give the maximum correlation of  $w_i$  with a linear combination of all the other EOS bins. The covariance matrix  $\mathbf{C}$  is the inverse of the Fisher matrix. The high redshift value  $w_3$  can either be fixed to the fiducial value (see §VI for consequences of the true value being different than the fiducial assumed) or marginalized over.

Figures 10 and 11 illustrate several interesting points. Both the bin positions and the treatment of  $w_3$  have a big impact on the uncertainties and correlations. Regarding the uncertainties, when  $w_3$  is kept fixed, the effect of making the first bin larger is to decrease  $\sigma_1$  (and increase  $\sigma_2$ ). (The slight rise in  $\sigma_1$  when the first bin gets very wide is due to covariance with the matter density and goes away with a tight  $\Omega_m$  prior.) They are of comparable size when the boundary between the two bins lies around  $z = 0.2$ . Note that there is only a very narrow region where the two parameters are determined to better than 0.1, so there is virtually no possibility of determining three EOS parameters to better than 0.1 with realistic next generation SN+CMB data – and this is in the most optimistic case of fixing  $w_3$ .

The correlation between estimates of  $w_1$  and  $w_2$  (still fixing  $w_3$ ) is not very strong, with minimum correlation at  $z_{\text{div}} \approx 0.5$ .

When the high redshift behavior of the dark energy EOS, represented by  $w_3$ , is not fixed a priori (after all, we want to probe dark energy properties, not assume them), significant changes occur. Examination of the global correlation coefficient for  $w_3$  shows this must happen:  $r_3$  ranges between 0.97 and 1, i.e. the high redshift behavior is extremely highly correlated with the low redshift behavior. This immediately tells us it that it is dangerous to fix  $w_3$  because if it is fixed to the wrong value, it can strongly affect the values derived for the other parameters (see §VI).

Another consequence of the strong correlation  $r_3$  is that including  $w_3$  as a fit parameter makes the uncertainties in  $w_1$  and  $w_2$  increase, by factors up to 10. When the first bin is small ( $z_{\text{div}} = 0.1$ ), it is hardly correlated with  $w_3$  and the change in its uncertainty is negligible, whereas  $\sigma_2$  is increased by a factor of almost four. However, as the boundary redshift is moved up, the first bin grows more correlated with the third bin until at  $z_{\text{div}} = 0.5$  both  $w_1$  and  $w_2$  have quite strong correlations with each other and with  $w_3$ , e.g.  $r_{13} = r_{23} = -0.99$ , and both  $\sigma_1$  and  $\sigma_2$  degrade considerably due to  $w_3$ . The effect is so strong that the trend of  $\sigma_1$  decreasing as the bin widens is broken:  $\sigma_1 = 0.33$  for  $z_{\text{div}} = 0.5$  compared to  $\sigma_1 = 0.09$  for  $z_{\text{div}} = 0.2$ .

Interestingly, when marginalizing over  $w_3$  there is a division redshift for which the estimations of the low redshift EOS values are uncorrelated,  $z_{\text{div}} \approx 0.18$ . This decorrelation, or pivot, redshift arises without any need for using the square root of the Fisher matrix. But for a broad choice of  $z_{\text{div}}$  the correlation is near unity. The strong correlation

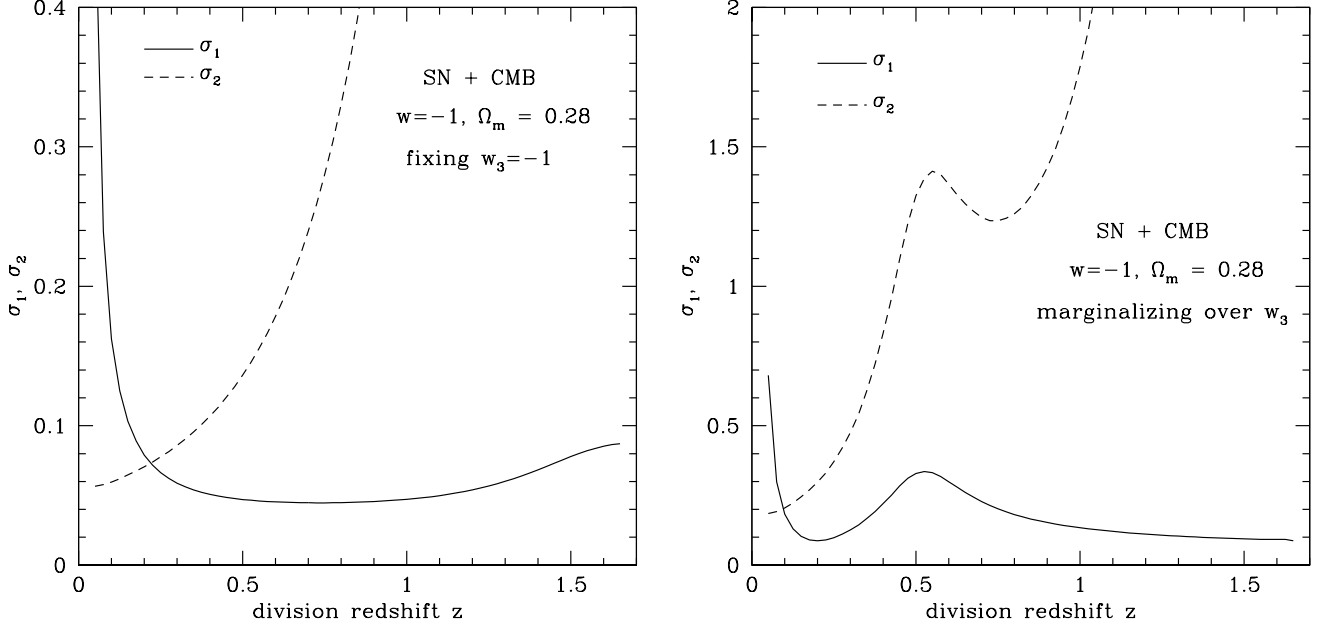


FIG. 10: Uncertainties in the EOS values for two bins between  $z = 0 - 1.7$  as a function of the redshift dividing the two bins. The first panel has fixed  $w_{N+1} = -1$ , the second panel has  $w_{N+1}$  marginalized over. Note the different scales.

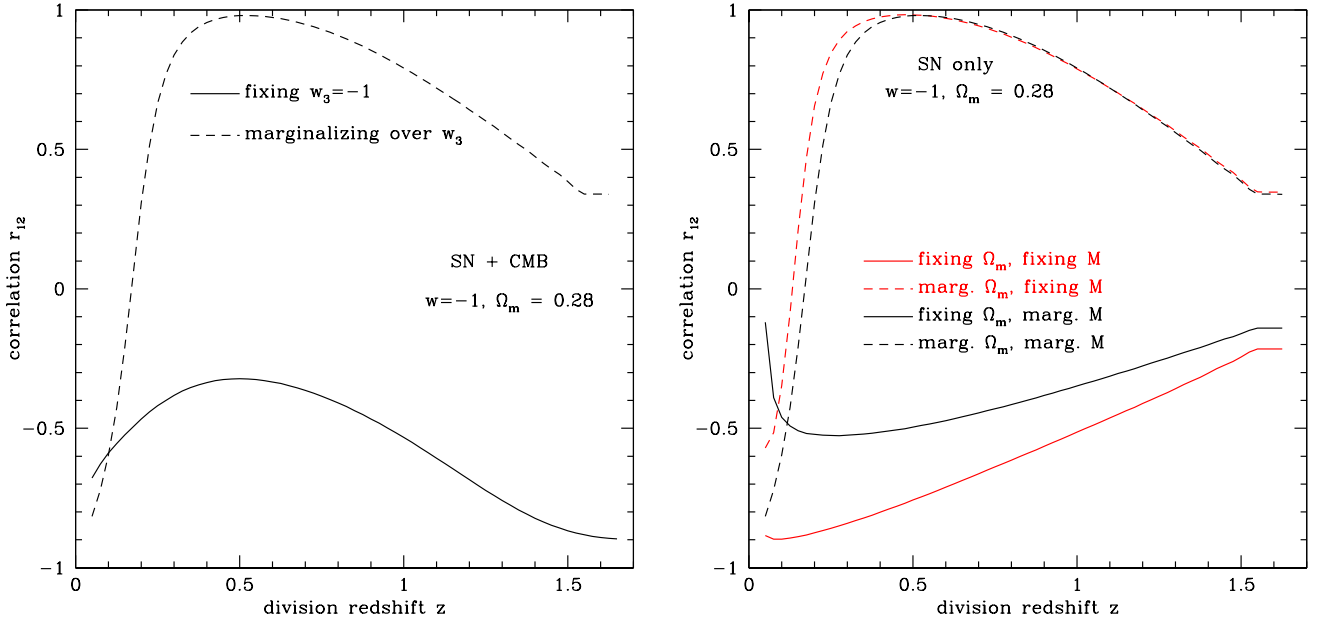


FIG. 11: As Fig. 10 but showing the correlation coefficient  $r_{12} = C_{12}/(\sigma_1\sigma_2)$  of the two  $z < 1.7$  bins as a function of the division redshift. The first panel uses SN and CMB data and compares fixing and marginalizing over  $w_{N+1}$ . The second panel shows that a tight prior on  $\Omega_m$  (without adding CMB data) has a similar effect on the correlations as adding CMB data and fixing  $w_{N+1}$ , i.e. one must be wary of priors dominating the behavior.

goes away when fixing  $w_3$ , but this is an example of prior information rather than data determining our view of the dark energy properties, as we saw in §IV B. For example, in the second panel of Fig. 11, we recreate the same behavior of breaking the strong correlation  $r_{12}$  by fixing  $\Omega_m$ . One must be cautious that priors do not overwhelm the data, to see a true picture of dark energy.

## B. Figures of Merit

In attempting to comprehend the nature of dark energy, some researchers advocate condensing the information down to a single figure of merit (FOM) related to the uncertainties in the parameter estimation. In §III we saw some difficulties of defining this in a robust manner. Indeed, FOM's for binned EOS typically depend sensitively on both the binning adopted (which has nothing to do with the cosmology within the data) and, again, the treatment of the high redshift EOS. We now analyze some possible FOM's for binned equations of state.

Figure 12, first panel, plots the area (taking out a factor  $\pi$ ) enclosed by the  $1\sigma$  confidence level contour in the  $w_1$ - $w_2$  plane, as a function of the bin division redshift. This area is proportional to  $(\det \mathbf{F})^{-1/2}$ , which is invariant under any transformation  $\mathbf{W}$  with  $(\det \mathbf{W})^2 = 1$  (see Eq. A4 or [22]), and in particular under any orthogonal transformation. When  $w_3$  is fixed (first panel), the area is minimized at a division redshift of  $z_{\text{div}} \approx 0.25$ . One might interpret this as saying that we obtain the most information (in the  $N = 2$  case) with one bin from  $z = 0 - 0.25$  and one from  $z = 0.25 - 1.7$ . When  $w_3$  is marginalized over, the behavior changes somewhat but there is still a clear minimum, this time at slightly lower redshift  $z_{\text{div}} \approx 0.18$ .

As more bins are added, individual bin parameters can become extremely uncertain and the volume  $(\det \mathbf{F})^{-1/2}$  in the  $N$ -dimensional space of  $w_1 \dots w_N$  (see, e.g., [23]) will be dominated by these poorly determined parameters. In an attempt to “cut off” the highly uncertain parameters, a figure of merit like

$$\text{FOM}_{\text{corr}} \equiv \sum_i \sigma_i^{-2} \quad (20)$$

has been proposed (see e.g. [16]).

We first consider the  $\sigma_i$  in Eq. (20) as the uncertainties in the (correlated) bin parameters  $w_i$ . The behavior of this FOM as a function of division redshift in the two bin case is shown in Fig. 12, second panel (note that now a large value is good). Such a measure would advocate – for the same data – using  $z_{\text{div}} \approx 0.65$  when  $w_3$  is fixed. In contrast, when  $w_3$  is marginalized, this peak in the FOM becomes a strong dip, saying the experiment is weak. Comparing to Fig. 10, this FOM can give high marks to choices that lose almost all the information on the second parameter.

The FOM discussed above does not take into account correlations between parameters. As an alternative, we could use the uncertainties in the *decorrelated* weighted averages  $\alpha'_i$  described in §IV. It is actually this choice, or rather its inverse, that is advocated in [16]. To be consistent with our previous notation, we should now write

$$\text{FOM}_{\text{decorr}} \equiv \sum_i \sigma_i'^{-2} \quad (21)$$

(note that this is the trace of the decorrelated Fisher matrix  $\mathbf{F}'$ ). This FOM has a very simple, but slightly disappointing interpretation:

$$\text{FOM}_{\text{decorr}} = \sigma(w)^{-2}, \quad (22)$$

i.e. the FOM is the inverse square uncertainty on a constant  $w$ , or equivalently when there is only one bin.<sup>2</sup>

---

<sup>2</sup> To see this, first note that in terms of the  $N$  decorrelated parameters  $\alpha'_i$ , the constant mode

$$e_{\text{const}}(z) = 1, \quad 0 < z < z_{\text{max}}, \quad (23)$$

which is the only mode present in the mode expansion when  $N = 1$ , is given by the  $N$ -dimensional vector  $\mathbf{e}'_{\text{const}} = (1, 1, \dots, 1)$  because the  $\alpha'_i$  are weighted averages of the original parameters. Hence, using the transformation law Eq. (A4) for the Fisher matrix, the diagonal element of the Fisher matrix corresponding to the coefficient of the constant mode (i.e. the Fisher information of the constant mode) is

$$\mathbf{e}'_{\text{const}}{}^T \mathbf{F}' \mathbf{e}'_{\text{const}} = \sum_{ij} F'_{ij} = \sum_i \sigma_i'^{-2}. \quad (24)$$

But by definition this quantity is the inverse variance of the coefficient of the constant mode in the case of  $N = 1$  bins.

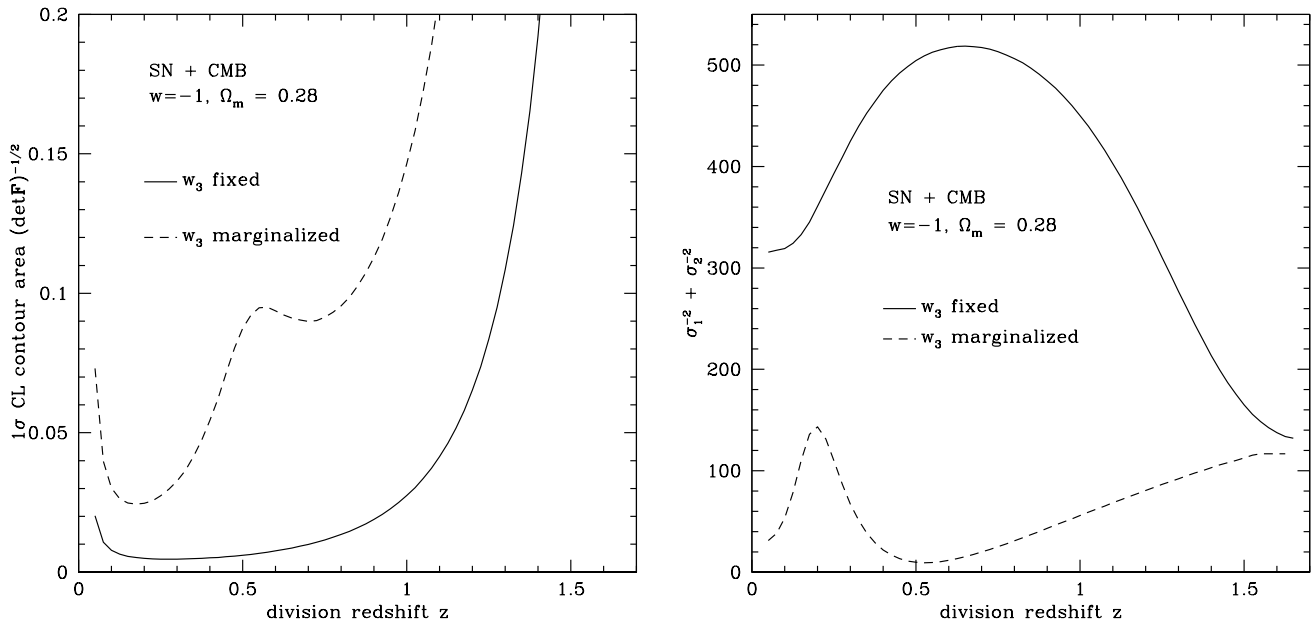


FIG. 12: As Fig. 10 but showing two suggested figures of merit. The first panel shows  $(\det \mathbf{F})^{-1/2} = A/\pi$  as a function of the bin division redshift  $z$ , where  $A$  is the area enclosed by the 68% confidence level contour in the  $w_1 - w_2$  plane for the model with two bins between  $z = 0$  and  $z = 1.7$ . The second panel shows  $\sum_i \sigma_i^{-2} = \sigma_1^{-2} + \sigma_2^{-2}$ .

We have confirmed numerically that, as it must be from the single bin interpretation, this trace FOM is independent of the division redshift(s) and number of bins. In conclusion, this FOM only captures the information that was already contained in the standard deviation of  $w$  when using the simplest parametrization, namely  $w = \text{constant}$ .

Note that neither the area (determinant) nor trace FOM's takes particular advantage of physical foundations. We have seen that the trace FOM neglects all dark energy dynamics, reducing to a constraint on a static EOS. For the area FOM, as discussed in [24], the area of the error contour is the Snarkian, or blank map, approach where all dynamics is equal. Instead, [24] advocates that the FOM must be adapted to the physics objective, e.g. whether one wants to distinguish the EOS from the cosmological constant or thawing behavior from freezing behavior, and depends on dark energy properties. We revisit physical bases for discerning the nature of dark energy in §VII.

## VI. HIGH REDSHIFT EQUATION OF STATE AND BIAS

For each method of analysis considered the high redshift value of the EOS has been shown to be a crucial ingredient; fixing the value of  $w_{N+1} = w(z > 1.7)$  has significant effects on the derived properties of the dark energy. A similar point has been made for functional forms by [25]. In addition to misestimating the uncertainties by fixing  $w_{N+1}$ , if it is fixed to the wrong value<sup>3</sup> (and a priori we don't know what the correct value is) then the *values* themselves of all the cosmological parameters are biased – we will derive a picture of dark energy skewed from reality.

Bias in derived parameters can be calculated from offsets in observables within the Fisher matrix formalism by (see, e.g., [24])

$$\delta p_i = (F^{-1})_{ij} \sum_k \frac{\partial O_k}{\partial p_j} \frac{1}{\sigma_k} \Delta O_k, \quad (25)$$

where  $\delta p_i$  is the difference of the estimated parameter value from its true value,  $\delta p_i \equiv p_{e,i} - p_{t,i}$ , and  $\Delta O_k$  is the offset in the  $k$ th observable. For bias arising from choosing the wrong value for  $w_{N+1}$  (which then propagates into

<sup>3</sup> Treating the EOS between  $z = 1.7$  and  $z = 1089$  as constant may introduce a bias in itself, but here we focus on the bias introduced by using the wrong constant value.



parameter $p_i$	$w_1 (z = 0 - 0.2)$	$w_2 (z = 0.2 - 0.5)$	$w_3 (z = 0.5 - 1.7)$	$w_4 (z = 1.7 - 1089)$	$\mathcal{M}$	$\Omega_{DE}$
PNGB true value	-0.83	-0.87	-0.93	-0.995	anything	0.72
$dp_i/dw_4$	-0.015	-0.019	-0.063	<b>x</b>	-0.00022	-0.0097
$\sigma(p_i)$ fixing $w_4$	0.10	0.16	0.15	<b>x</b>	0.016	0.012
parameter $p_i$	$w_1 (z = 0 - 0.2)$	$w_2 (z = 0.2 - 0.5)$	$w_3 (z = 0.5 - 1.7)$	$w_4 (z = 1.7 - 1089)$	$\mathcal{M}$	$\Omega_{DE}$
Bending true value	-0.84	-0.72	-0.55	-0.16	anything	0.72
$dp_i/dw_4$	-0.21	-0.26	-0.39	<b>x</b>	-0.0022	-0.14
$\sigma(p_i)$ fixing $w_4$	0.096	0.16	0.11	<b>x</b>	0.016	0.012

TABLE I: Biases in cosmological parameter estimation due to fixing  $w(z > 1.7)$  to an incorrect value. The top half of the table considers a PNGB dark energy model, which has  $w(z > 1.7) \approx -1$ , and the bottom half considers a bending dark energy model, where  $w(z > 1.7)$  differs substantially from  $-1$ . The amount of bias  $dp_i$  per how much  $w_4$  is misestimated is shown in the middle row of each set.

the expected, i.e. simulated, observation), the expression becomes (see Appendix C)

$$\frac{dp_i}{dp_{N+1}} = - \sum_{j=1}^N (F^{(N)})_{ij}^{-1} (F^{(N+1)})_{j,N+1}, \quad (26)$$

where  $dp_{N+1}$  is the difference of the value  $w_{N+1}$  is fixed to from its true value,  $\delta p_{N+1} = p_{\text{fix},N+1} - p_{t,N+1}$ .

To give concrete examples of the induced parameter bias, we choose two EOS models that we will fit with binned piecewise constant EOS. We use three low redshift bins  $z = 0 - 0.2$ ,  $0.2 - 0.5$ ,  $0.5 - 1.7$  and a high redshift bin from  $z_{\text{max}} = 1.7$  to  $z_{\text{iss}} = 1089$ , and define a weighted average

$$w_{N+1} = \frac{1}{\Delta \ln(1+z)} \int_{z_{\text{max}}}^{z_{\text{iss}}} \frac{dz}{1+z} w(z). \quad (27)$$

(For consistency, we use an appropriately defined weighted average for each bin.)

The first model is based on a pseudoNambu-Goldstone boson (PNGB) model [26], which has  $w_{N+1} \approx -1$ ,

$$w(z) = -1 + (1 + w_0)(1 + z)^{-F} \quad (28)$$

with  $w_0 = -0.8$  and  $F = 1.5$ . The second model is based on a so called bending model [27] motivated by dilaton fields, giving a nonnegligible contribution of early dark energy density (here  $\sim 2\%$  relative to the matter density) and  $w_{N+1}$  far from  $-1$ :

$$w(z) = \frac{w_0}{[1 + b \ln(1 + z)]^2}, \quad (29)$$

with  $w_0 = -0.9$  and  $b = 0.415$  (this is very similar to the model  $w(z) = w_0 + w_a(1 - a)$ , with  $w_0 = -0.9$  and  $w_a = 0.7$ ). In both cases,  $\Omega_m = 0.28$ .

Table I shows the EOS values in each bin for both models and also the amount of bias of the estimated parameter values per offset of  $w_{N+1}$  relative to the a priori assumption, as calculated from Eq. (26). For example, if one assumed that  $w_{N+1} = -1$ , then the bias in  $w_2$  for the bending model would be  $\delta w_2 = 0.22 = -0.26 \times (-1 + 0.16)$ ; that is, instead of measuring the true value  $w_2 = -0.72$  one would think  $w_2 = -0.50$ . Assuming cosmological constant behavior at high redshift has very little effect on the PNGB model, since at high redshift it indeed is close to  $w = -1$ . But we don't know a priori what the true dark energy behavior will be.

To avoid bias, we must leave  $w_{N+1}$  as a fit parameter. However, this greatly increases the uncertainties, since adding a single parameter and a single data point, with only that data point constraining that parameter, is equivalent to adding neither the parameter nor the data as far as the uncertainties in the original parameters are concerned – essentially throwing away the high redshift bin. The solution that allows for control of both bias and uncertainty is to obtain more, useful data that depends on  $w_{N+1}$ . Such data could be higher redshift distances, such as from baryon acoustic oscillation (BAO) measurements using quasars or the Lyman alpha forest, or from matter density growth factors such as enter into weak gravitational lensing measurements. While we note that SNAP, which we took to provide the supernova sample, includes highly precise weak lensing measurements, here we continue to concentrate on distances and illustrate the effect of a 1.2% measurement of the reduced angular distance  $\tilde{d}$  (transverse BAO scale) at  $z = 3$  such as the BOSS experiment [28] could provide.

<b>PNGB</b>	$\sigma_1$	$\sigma_2$	$\sigma_3$	$\sigma_4$	$r_{12}$	$r_{13}$	$r_{14}$	$r_{23}$	$r_{24}$	$r_{34}$
fixing $w_4$	0.10	0.16	0.15	<b>x</b>	-0.76	0.45	<b>x</b>	-0.72	<b>x</b>	<b>x</b>
fitting $w_4$ (CMB)	0.32	0.42	1.3	20	0.79	0.96	-0.95	0.89	-0.92	-0.99
fitting $w_4$ (CMB+ $d_3$ )	0.10	0.16	0.17	2.1	-0.73	0.48	-0.21	-0.59	-0.13	-0.53
<b>Bending</b>	$\sigma_1$	$\sigma_2$	$\sigma_3$	$\sigma_4$	$r_{12}$	$r_{13}$	$r_{14}$	$r_{23}$	$r_{24}$	$r_{34}$
fixing $w_4$	0.096	0.16	0.11	<b>x</b>	-0.73	0.39	<b>x</b>	-0.84	<b>x</b>	<b>x</b>
fitting $w_4$ (CMB)	0.98	1.2	1.8	4.7	0.98	1.00	-1.00	0.98	-0.99	-1.00
fitting $w_4$ (CMB+ $d_3$ )	0.098	0.15	0.12	0.07	-0.77	0.43	-0.20	-0.81	0.20	-0.48

TABLE II: As Table I, showing the EOS uncertainties and correlation coefficients. Fitting for  $w_4 \equiv w(z > 1.7)$ , which removes the bias calculated in Table I, increases the uncertainties and correlations, but the addition of further high redshift data (here illustrated with  $d_3 \equiv \tilde{d}(z = 3)$ ) can substantially restore them.

Table II shows the effects on the EOS uncertainties from fixing  $w_{N+1}$  (and so incurring bias), fitting for it with only a CMB  $d_{\text{ISS}}$  measurement (and so effectively using SN alone), and fitting for it with both  $d_{\text{ISS}}$  and  $\tilde{d}(z = 3)$  measurements. We see that not only do the uncertainties greatly decrease when data give constraints on the high redshift expansion history, but the correlations between EOS parameters greatly diminish. Again we emphasize that weak lensing measurements have the same or better effect. The key point is that assuming high redshift behavior for dark energy leads to bias – to overcome this requires accurate measurements (beyond CMB data alone) of the high redshift universe, e.g. through direct  $z > 1.7$  observations or through weak lensing observations involving the growth factor. Given such measurements, one recovers almost the full leverage on the EOS as when  $w_{N+1}$  was assumed, but without bias. For the two very different models we considered, the EOS parameter estimation by doing a global fit including  $w_{N+1}$  is degraded by less than 15% and the risk (the uncertainty and the bias summed in quadrature) is improved by factors up to 3. Of course if with the additional data one attempts to fit additional high redshift EOS parameters, then the constraints do not improve as much.

## VII. PHYSICAL CONSTRAINTS ON EQUATION OF STATE

### A. Eigenmode Expansion

We pointed out at the end of §III that to reduce the parameter space by throwing out poorly determined modes in the eigenmode expansion, we need to make assumptions about the appropriate range of values for the parameters/coefficients  $\alpha_i$ . One way to do this is to take constraints on  $w(z)$  based on theory (if we have any such constraints) and convert these into constraints on the parameters  $\alpha_i$  (see for example [5]). If for example we then find that  $-\alpha_i^{\text{max}} < \alpha_i < \alpha_i^{\text{max}}$ , we may want to throw out the  $i$ th mode if  $\alpha_i^{\text{max}} < \sigma_i$  (or perhaps  $\alpha_i^{\text{max}} < 2\sigma_i$ ) because  $\alpha_i^{\text{max}} = \sigma_i$  means that the maximum physical signal in  $\alpha_i$  is equal to its observational uncertainty and thus we cannot get a convincing signal in this parameter.

As an example, imagine we expect the equation of state to be  $w = -1$  and have some reason to believe that  $-2 < w(z) < 0$  is required, for all  $z$ . In other words, if we choose the baseline equation of state (see Eq. 2) to be  $w_b = -1$ , we want the magnitude of the deviation from the baseline to be smaller than one:

$$|w(z) - w_b(z)| = \left| \sum_i \alpha_i e_i(z) \right| < 1. \quad (30)$$

This constraint of course defines some complicated volume in the  $\alpha_1 \dots \alpha_N$  space (correlating the constraints on the different  $\alpha_i$ ), but we can get simple maxima  $\alpha_i^{\text{max}}$  for the individual  $\alpha_i$  by treating the constraint (30) less rigorously.

One way of doing this is to demand that the contributions of the individual modes do not exceed one, i.e.  $|\alpha_i e_i(z)| < 1$  for all  $z$  for each  $i$  individually. This gives

$$\alpha_i^{\text{max}} = 1/|e_i(z)|_{\text{max}} \quad (31)$$

and we have checked that (using the criterion  $\alpha_i^{\text{max}} < \sigma_i$ ) this allows us to throw out all but the first five modes for the case depicted in Fig. 4 (left), independent of whether the binning is uniform in  $z$ ,  $a$  or  $\ln(1+z)$ . One of the problems with this approach is that if one mode locally causes an unacceptably large deviation from  $w = -1$ , this deviation

may be canceled by another mode with large amplitude so in those cases the constraint is stricter than Eq. (30). The inverse is also true, that a mode that has an acceptably small deviation might be augmented by another mode so as to exceed our desired constraint.

An alternative approach that does not suffer from the first of the two problems mentioned above is discussed in §3 of [13], where it is applied to the reionization history of the universe instead of the dark energy EOS (note the ionization fraction is bounded in  $[0,1]$ ). In this approach, maxima are calculated such that if *any* coefficient violates  $|\alpha_i| < \alpha_i^{\max}$ , Eq. (30) is violated as well. The converse is not true. All modes satisfying  $|\alpha_i| < \alpha_i^{\max}$  does not guarantee that the original constraint is satisfied so this approach does suffer from the second problem mentioned in the previous paragraph. The  $\alpha_i^{\max}$ 's calculated in this approach are greater than (or equal to, in the limiting case of a constant mode) the ones in the approach discussed above and thus give a larger range of allowed values. When applied to the case at hand, the maxima for the approach discussed in [13] are given by

$$\alpha_i^{\max} = \int dz |e_i(z)|. \quad (32)$$

We have checked, again for the case depicted in Fig. 4 (left), that if we require this  $\alpha_i^{\max} > \sigma_i$  then this very conservative criterion means we can eliminate modes beyond the first 9 or 10 (depending on if we calculate the eigenmodes with respect to  $z$ ,  $a$  or  $\ln(1+z)$ ).

Note that even if we throw out a large number of modes using the methods described above, the remaining parameters still carry a lot of uncertainty. Also, to illustrate our ideas we have assumed an expected  $w = -1$  with  $-2 < w(z) < 0$ , but in reality we have very little knowledge to base such assumptions on (but see the next subsection). Finally, please recall that in §III we identified two main problems with the eigenmode approach. Above, we considered the problem of how to quantify which modes are well-determined and which ones are not. However, there was another problem, namely that different binnings give a different set of modes. This implies that, after throwing out poorly determined modes, essentially different models remain. For example, the first five modes with respect to  $a$  span a different set of equations of state than the first five modes with respect to  $z$ .

## B. Time Variation

The EOS  $w(z)$  has physical constraints not just on its value but also its time variation. The effective mass of scalar field dark energy is related to the curvature of the potential and can be written in terms of  $w$ ,  $w'$ , and  $w''$ , as in [29, 30], where a prime denotes a derivative with respect to  $\ln a$ . (Note there is a typo in the first term of Eq. 46 in [30] where  $2q$  should be  $q/2$ .) If the mass exceeds the Hubble parameter,  $m \gg H$ , then the Compton wavelength for fluctuations in the scalar field will be less than the Hubble length and dark energy will exhibit clustering [31]. If we wish to disallow such models (ideally through observational constraints, although high energy physics such as supergravity can lead to limits on mass scales [32]) then this imposes the condition

$$\frac{m}{H} \lesssim 1 \quad \implies \quad \left| \frac{w'}{1+w} \right| \lesssim 1, \quad (33)$$

unless the relation between  $w$ ,  $w'$ , and  $w''$  is fine tuned. For example, this imposes constraints on oscillatory behavior, saying the variation cannot be too extreme. For EOS expanded in a Fourier basis in  $\ln a$ , say, all terms  $\cos(B \ln a)$  with  $B \gg 1$  would give inhomogeneities so the physical condition of smoothness would limit which modes should be included.

In terms of binned EOS, the condition (33) reads

$$\left| \frac{w_{i+1} - w_i}{1 + (w_{i+1} + w_i)/2} \right| \frac{1}{\ln[(1+z_{i+1})/(1+z_i)]} \lesssim 1. \quad (34)$$

To help satisfy this we want a large distance between bin centers. Taking the extreme case of  $z_1 \approx 0$ ,  $z_2 \approx 1.7$ , then  $|\Delta w| \lesssim 1 + \bar{w} \lesssim 1$ . That is, bin values should not jump by of order unity. For bins closer together the jump constraint is tighter. Dark energy lying within the thawing and freezing regions defined by [33] automatically satisfies the mass constraint. For effective dark energy without a physical fluid, as in extended gravity origins, constraints on  $w'$  from inhomogeneity considerations may not apply. Other possibilities for constrained EOS behavior can arise within a particular class of models; [34] explores this for some potentials using PCA and [2] chooses a correlation function over redshift for  $w(z)$ .

$\sigma(w_2 - w_1)$	$\sigma(w_3 - w_2)$	$\sigma(w_3 - w_1)$	$\sigma(w_4 - w_3)$	$\sigma(w_4 - w_2)$	$\sigma(w_4 - w_1)$	$\sigma(w'_{12})$	$\sigma(w'_{23})$	$\sigma(w'_{34})$
0.47	0.94	0.57	0.88	0.36	0.35	2.8	6.6	2.4

TABLE III: Uncertainties in the EOS jumps between bins and the derivatives  $w' \equiv dw/d \ln a$  for the four redshift bins covering  $z < 1.7$  of Eq. (16). Note  $w_{N+1}$  is fixed to  $-1$ .

### C. Testing the Equation of State

Finally, one might want to apply several tests for physical properties to the EOS, which can be phrased simply in terms of the EOS bin values. To check consistency with the cosmological constant,  $w = -1$ , to a confidence level of  $S\sigma$ , one looks for  $(1 + w_i)/\sigma(w_i) > S$ . To look for departures from a constant EOS, one probes whether

$$\frac{w_i - w_j}{\sigma(w_i - w_j)} = \frac{w_i - w_j}{\sqrt{\sigma_i^2 + \sigma_j^2 - 2C_{ij}}} > S, \quad (35)$$

for any  $i, j$ . This also gives a necessary but not sufficient condition for distinguishing thawing vs. freezing behavior: whether  $w$  decreases or increases with larger redshift.

Another interesting property would be nonmonotonicity in the EOS. This could be indicated by having  $w_{i+p} - w_i$  of opposite sign from  $w_{i+r} - w_{i+q}$ , where  $p < q < r$ . (Note we do not only consider consecutive bins since low  $\sigma$  differences between neighboring bins could add up to statistically significant deviations over a wider range.) That is, one tests whether

$$\frac{w_{i+p} - w_i}{\sigma(w_{i+p} - w_i)} < -S \quad \text{and} \quad \frac{w_{i+r} - w_{i+q}}{\sigma(w_{i+r} - w_{i+q})} > S, \quad (36)$$

or the opposite.

While from the above points it would appear that for testing  $\Lambda$ , say, the FOM should be minimizing  $\sigma(w_i)$  in any one bin, this in fact does not hold. Such a criterion would drive us to create a single bin over the entire data redshift range, indeed giving a minimal  $\sigma(w_i)$ , but erasing any dynamics, taking a constant  $w$ . This averaged  $w$  can in fact under certain circumstances be driven to appear as  $w = -1$  despite real time variation [25], so such a FOM is not useful. For checking constancy, monotonicity, and related properties, one might advocate a FOM involving  $\sigma(w_{i+p} - w_i)$ . This effectively takes a further derivative of the cosmological expansion and tends to yield large errors (while of course being a highly unstable procedure if applied directly to the data).

Table III demonstrates the lack of precision in determining  $w_{i+p} - w_i$  or the variation  $w' = dw/d \ln a$ , even when fixing the high redshift behavior  $w_{N+1}$  (*not* recommended), within the binned EOS approach. Even for this optimistic case with next generation data, fitting four EOS parameters is too much: the dynamics represented by  $w'$  cannot be seen. This agrees with [18] that next generation data will only allow physical insight into two EOS parameters. For the two bin case we considered in §V, one can obtain  $\sigma(w'_{12}) = 0.23$ .

## VIII. CONCLUSIONS

The dark energy equation of state properties contain clues crucial to understanding the nature of the acceleration of the cosmic expansion. Deciphering those properties from observational data involves a combination of robust analysis and clear interpretation. We considered three approaches – principal components, uncorrelated bandpowers, and binning; none of the approaches provides a panacea.

In particular, we identify issues of dependence on basis functions, binning variables, and baseline models. The three approaches are not truly nonparametric and physical interpretation (not merely the values) of the results in the two decorrelated basis techniques depends on model, priors, and data, indeed even on an implicitly assumed functional form. Nevertheless, principal components can give a useful guide to the qualitative sensitivity, the best constrained aspects, of the data.

The uncorrelated bin approach unfortunately does not truly deliver uncorrelated bandpowers for the equation of state. This approach using the square root of the Fisher matrix does not tightly localize the information (without a strong prior), making the interpretation nontrivial. This property of nonlocality is inherent in the cosmological characteristics. One might prefer to stay with the original binned equations of state used as the initial step for this technique, which are readily interpreted. Conversely, if the modes can be localized, the interpretation is easy, but in

that case the original Fisher matrix is close to diagonal and thus the original bins almost uncorrelated. Hence, again, one might as well stay with the bin parameters which have a clear meaning.

Indeed the goal is understanding the physics, not obtaining particular statistical properties. Decorrelated parameters that are not readily interpretable physically are of limited use; for example one still prefers to analyze the cosmic microwave background in terms of physical quantities such as physical matter density and spectral tilt rather than the principal axes of the eigenvectors. Note that the uncertainty on the EOS behavior  $\sigma(w(z))$  is the same whether calculated by PCA (if all modes are kept), uncorrelated bands, or binned EOS, since the same information is in the data. We also emphasize that the modes most clearly determine the effect on the equation of state, not the weights, which are often the only quantity displayed. Moderately localized, even all positive, weights do not guarantee a localized physical effect. A further caution is that locality and positivity of weights can owe more to prior restrictions, especially the treatment of the high redshift equation of state, than to the data itself.

Assuming a fixed value for the high redshift equation of state has major, widespread impacts on the results, ranging from strongly misestimated uncertainties to spurious localization to bias in the derived cosmology. We emphasize that it is essential to fit for the high redshift behavior in order not to be misled. Adding CMB data and marginalizing over a new, high redshift bin removes the ill effects of bias but “cancels out”, providing no new constraints; multiple data points for  $z > 2$  are required, such as from high redshift distances or weak lensing measurements of the mass growth behavior. Assuming that dark energy is negligible at  $z > 2$  is also effectively assuming a functional form – precisely what the use of eigenmodes was supposed to avoid.

Indeed, functional forms do not have many of the basis, model, binning, etc. dependences of eigenmodes, while principal components are in turn not fully form independent. If one assumes a functional form to obtain informative constraints on the equation of state, one must indeed choose the form to represent robustly the physical behavior (as has been shown to be widely the case for  $w(a) = w_0 + w_a(1 - a)$  by [25, 35]), and carefully check the range of validity of the conclusions by examining other forms. A good complementary analysis tool would be the binned equation of state approach examined here.

Regardless of the form of analysis, only a finite amount of information can be extracted from even next generation data. As has been concluded for functional equations of state and principal component analysis [18], the analysis here in terms of binned equation of state indicates that only two physically informative parameters can be fit with realistic accuracy. However, we identify several issues in the PCA and uncorrelated bin approaches that cause accuracy or signal to noise criteria to be ill defined. Similar difficulties arise in condensing the physical information on dark energy to a single figure of merit; the number is quite sensitive to cosmologically irrelevant aspects like the binning used (as well as very dependent on the treatment of the high redshift dark energy behavior).

In conclusion, physically motivated fitting of the equation of state such as the  $w_0-w_a$  parametrization in complement with a binned equation of state approach (perhaps with physical constraints such as outlined in §VII) have the best defined, clearest to interpret, and robust insights of the approaches we considered. With any method, one must use caution regarding the influence of priors and fit the dark energy physics over the entire expansion history.

### Acknowledgments

We thank Dragan Huterer for helpful discussions. This work has been supported in part by the Director, Office of Science, Department of Energy under grant DE-AC02-05CH11231.

## APPENDIX A: PROPERTIES OF DECORRELATED MODES

In this Appendix, we first introduce some definitions and discuss some useful general properties of decorrelated modes (§A 1). We then show that eigenvectors are formally ill-defined for a Fisher matrix (§A 2) and that the eigenmodes (eigenvectors in the limit of a large number of bins) depend on the coordinate (redshift  $z$ , scale factor  $a$ , etc.) one uses to write the EOS  $w$  as a function of (§A 3). We consider the latter to be the main result of this Appendix.

### 1. Basis Expansion

The matrix  $\mathbf{W}$  defines a basis transformation by

$$\mathbf{e}'_i = W_{ij} \mathbf{e}_j, \quad (\text{A1})$$

so that the rows of  $\mathbf{W}$  contain the new basis vectors as expressed with respect to the old basis<sup>4</sup>. The coefficients, or components,  $\alpha = (\alpha_1, \dots, \alpha_N)$  then transform according to

$$\alpha' = (\mathbf{W}^{-1})^T \alpha. \quad (\text{A2})$$

If the transformation is orthogonal,  $\mathbf{W}^T = \mathbf{W}^{-1}$ , the basis vectors and the coefficients transform in the same way. However, this is not the case in general.

Since the Fisher matrix is a Hessian matrix, i.e. it is defined in terms of second order partial derivatives,

$$F_{ij} = \left\langle -\frac{\partial^2 \ln L}{\partial \alpha_i \partial \alpha_j} \right\rangle, \quad (\text{A3})$$

it transforms according to

$$\mathbf{F}' = \mathbf{W} \mathbf{F} \mathbf{W}^T. \quad (\text{A4})$$

It will become clear below that one of the main points of §III, namely that eigenmodes depend on the binning used to calculate them in, is essentially a consequence of this transformation behavior.

Diagonalizing  $\mathbf{F}$  comes down to finding a matrix  $\mathbf{W}$  such that

$$\mathbf{W} \mathbf{F} \mathbf{W}^T = \mathbf{D} \quad (\text{A5})$$

is diagonal. In such a basis the uncertainties in the coefficients  $\alpha'_i$  are uncorrelated. It is straightforward to show that there is an infinite number of bases that achieve this. The remainder of this Appendix focuses on the particular choice of eigenvectors as basis (see also §III).

## 2. Basis Dependence of Eigenmodes

If a set of eigenvectors is orthonormal (which can always be arranged), the eigenvalues are equal to the diagonal elements of the diagonal Fisher matrix, i.e. the inverse variances. Eigenvectors are defined by

$$\mathbf{F} \mathbf{v} = \lambda \mathbf{v}, \quad (\text{A6})$$

and their components transform according to Eq. (A2). However, since the Fisher matrix transforms according to Eq. (A4), this is not a covariant statement:

$$\mathbf{F}' \mathbf{v}' = \mathbf{W} \mathbf{F} \mathbf{W}^T (\mathbf{W}^{-1})^T \mathbf{v} = \lambda \mathbf{W} \mathbf{v}. \quad (\text{A7})$$

This is only equal to

$$\lambda \mathbf{v}' = \lambda (\mathbf{W}^{-1})^T \mathbf{v} \quad (\text{A8})$$

if the coordinate transformation is orthogonal, i.e.  $\mathbf{W}^T = \mathbf{W}^{-1}$ , but not in general! This means that, formally, eigenvectors of a Fisher matrix are not well-defined.

Of course, we can take a pragmatic approach and just compute the eigenvectors (for lack of a better word, we will still call them eigenvectors) in a particular basis and work with those. This is what we will do, but it is important to remember that the set of eigenvectors found in this way depends on the particular basis we chose to compute them in.

## 3. Coordinate Dependence of Eigenmodes

We now turn our attention to the eigenmodes in the  $N \rightarrow \infty$  limit, where  $N$  is the number of EOS bins. We start with the basis of modes  $e_i(z)$  discussed in §II that are equal to one inside the  $i$ th bin and zero everywhere else. In

---

<sup>4</sup> Note that in some literature (e.g. [14, 15]) the transformation matrix is defined as the matrix transforming the coordinates: our  $\mathbf{W}$  is the inverse transpose of that matrix.

the limit  $N \rightarrow \infty$  (keeping the *relative* bin widths the same) the eigenvectors approach a set of continuous functions (eigenmodes) and these eigenmodes and the corresponding standard deviations converge (see for example [1]).

In this section, we address the question of whether the eigenmodes are independent of which coordinate we use to write  $w$  as a function of. For example, we may choose a binning that is uniform in terms of the scale factor  $a = 1/(1+z)$ , i.e.  $\Delta a$  constant instead of uniform in  $z$ , i.e.  $\Delta z$  constant. Note that this is equivalent to a non-uniform binning in  $z$ ,

$$\Delta z_i \approx \frac{dz}{da}(z_i) \Delta a, \quad (\text{A9})$$

where  $z_i$  is a redshift inside the  $i$ th bin. Since we saw before that eigenvectors of the Fisher matrix are basis dependent, it should not be too surprising if the eigenmodes turn out to depend on the relative bin sizes. Indeed, we find this is the case. We will explain this in the remainder of this section (specific examples are shown in §III).

Assume a binning that is uniform in a variable  $x = x(z)$ , which is either monotonically increasing or decreasing as a function of  $z$  in the relevant redshift range. For example,  $x$  could be the scale factor  $a$  or perhaps its logarithm. To see if the eigenmodes calculated using  $x$  are the same as the ones calculated using  $z$ , we will need to make use of the following results.

Let  $\mathbf{F}$  be the Fisher matrix for a set of  $N$  bins with widths  $\Delta z_i$  and  $\mathbf{F}'$  be the one for a set of  $N'$  bins with widths  $\Delta z'_i$ . Then for large enough  $N$  and  $N'$ ,

$$F'(z, z') \approx \frac{\Delta z'}{\Delta z}(z) \frac{\Delta z'}{\Delta z}(z') F(z, z'), \quad (\text{A10})$$

where we have replaced discrete indices by the redshifts of the corresponding bins. For example,  $F(z, z') \equiv F_{ij}$  where the  $i$ th bin contains  $z$  and the  $j$ th bin contains  $z'$ . Eq. (A10) follows from the fact that derivatives with respect to EOS bin parameters should scale with the bin width for small enough bins. If we apply the above result to the cases of a binning with  $\Delta z$  constant and one with  $\Delta x$  constant, we get

$$F^{(x)}(z, z') \approx \left(\frac{\Delta x}{\Delta z}\right)^2 \frac{dz}{dx}(z) \frac{dz}{dx}(z') F^{(z)}(z, z'), \quad (\text{A11})$$

where the superscript on  $F$  denotes in which binning the Fisher matrix is calculated.

We can now apply the results from the previous paragraph to the eigenmodes discussion. Let us assume that  $v(z)$  is an eigenmode calculated using  $z$ , i.e.

$$\sum_{z'(\Delta z)} F^{(z)}(z, z') v(z') = \lambda v(z), \quad (\text{A12})$$

where the  $(\Delta z)$  below the summation symbol indicates that the sum is supposed to be carried out over the bins (labeled by  $z'$ ) uniformly spaced in  $z$ . Then,

$$\begin{aligned} \sum_{z'(\Delta x)} F^{(x)}(z, z') v(z') &= \left(\frac{\Delta x}{\Delta z}\right)^2 \sum_{z'(\Delta x)} \frac{dz}{dx}(z) \frac{dz}{dx}(z') F^{(z)}(z, z') v(z') \\ &= \left(\frac{\Delta x}{\Delta z}\right)^2 \sum_{z'(\Delta z)} \frac{\Delta z}{\Delta x} \frac{dx}{dz}(z') \frac{dz}{dx}(z) \frac{dz}{dx}(z') F^{(z)}(z, z') v(z') \\ &= \frac{\Delta x}{\Delta z} \frac{dz}{dx}(z) \sum_{z'(\Delta z)} F^{(z)}(z, z') v(z') \\ &= \lambda \frac{\Delta x}{\Delta z} \frac{dz}{dx}(z) v(z), \end{aligned} \quad (\text{A13})$$

where in the first equality we have used Eq. (A11), in the second equality we went from the binning uniform in  $x$  to the binning uniform in  $z$ , which forced us to put in a factor  $\frac{\Delta z}{\Delta x} \frac{dx}{dz}(z')$ , and in the fourth equality we use the fact that  $v(z)$  is an eigenmode in the binning uniform in  $z$ , i.e. Eq. (A12). What the above shows is that  $v(z)$  is an eigenmode in the  $x$ -binning only if  $\frac{dz}{dx} = \text{const}$  (recall that  $\Delta x$  and  $\Delta z$  are just constants by construction). Hence, using the scale factor  $a$  or any other coordinate that is not a linear function of  $z$  will result in a different set of eigenmodes. (We illustrate this with numerical results in Fig. 4 of §III A). The above has strong implications when we try to decide how many modes/parameters are well determined, an issue that is explored further in §VII A.

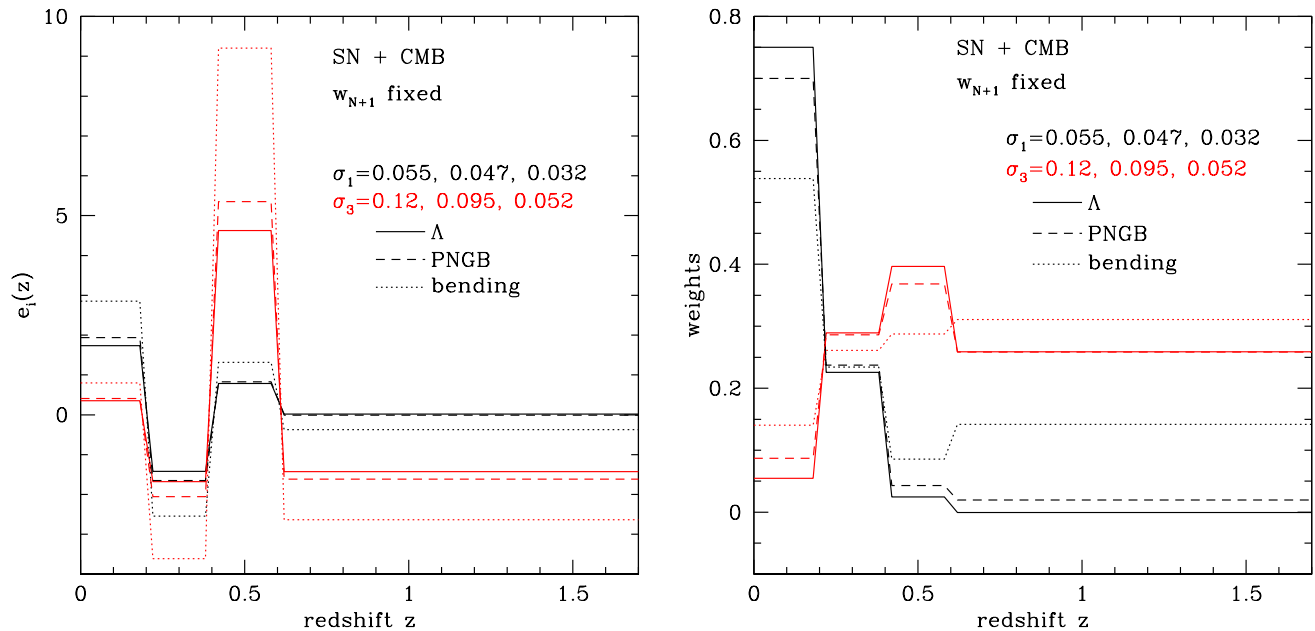


FIG. 13: As Fig. 5, but comparing the first and third modes (left panel) and associated weights (right panel) for three dark energy fiducial models: cosmological constant  $\Lambda$ , PNGB, and bending (see §VI). Here we fix  $w_{N+1}$  to its appropriate fiducial value for each model.

## APPENDIX B: MODEL DEPENDENCE

In addition to the modes and weights depending on basis, binning variable, and specific binning choice, we now consider dependence on the fiducial model. We analyze how the uncorrelated bandpowers that were discussed in §IV change as the fiducial EOS is changed from the  $w = -1$   $\Lambda$ CDM cosmology to the (discretized) PNGB and bending models discussed in §VI.

Figures 13 and 14 show how the first and third modes, the corresponding weights, and the uncertainties change between these models. We again show results both for the case where we fix the EOS at  $z > 1.7$  to the respective fiducials (Fig. 13) and for the case where we treat it as a free parameter (Fig. 14). While the PNGB results lie rather close to the  $\Lambda$ CDM ones, the bending model results in significantly different bandpowers and uncertainties. Fiducial models deviating appreciably from each other will induce appreciable model dependence in the mode analysis. Note that changing the fiducial does not make the weights look “better”, i.e. they do not get significantly more localized or positive.

## APPENDIX C: PARAMETER BIAS FORMULA

In this section we derive Eq. (26), which tells us how much we misestimate the other parameters when we fix one of the parameters to the wrong value. Consider the general case where the observables  $O_k = O_k(\{p_i\}_{i=1}^{n+1})$  depend on  $n + 1$  parameters  $p_i$ . We call the true values of the parameters  $p_{t,i}$ . Now imagine that, instead of fitting all  $n + 1$  parameters to the data, we first fix  $p_{n+1}$  to  $p_{\text{fix},n+1}$  and then fit the resulting  $n$  parameters to the data. To get the correct values for these parameters, the observables would have to be given by  $O_k(\{p_{t,i}\}_{i=1}^n, p_{\text{fix},n+1})$ . In reality, ignoring observational uncertainties (we do not want to write “the expectation values of” over and over), the data are given by  $O_k = O_k(\{p_{t,i}\}_{i=1}^{n+1})$ . Hence, if  $p_{\text{fix},n+1} \neq p_{t,n+1}$ , the  $n$  parameter values  $p_{e,i}$  derived from the data will be different from the actual values.

If we define

$$\Delta O_k \equiv O_k(\{p_{t,i}\}_{i=1}^{n+1}) - O_k(\{p_{t,i}\}_{i=1}^n, p_{\text{fix},n+1}) = -\frac{\partial O_k}{\partial p_{n+1}} \delta p_{n+1}, \quad (\text{C1})$$



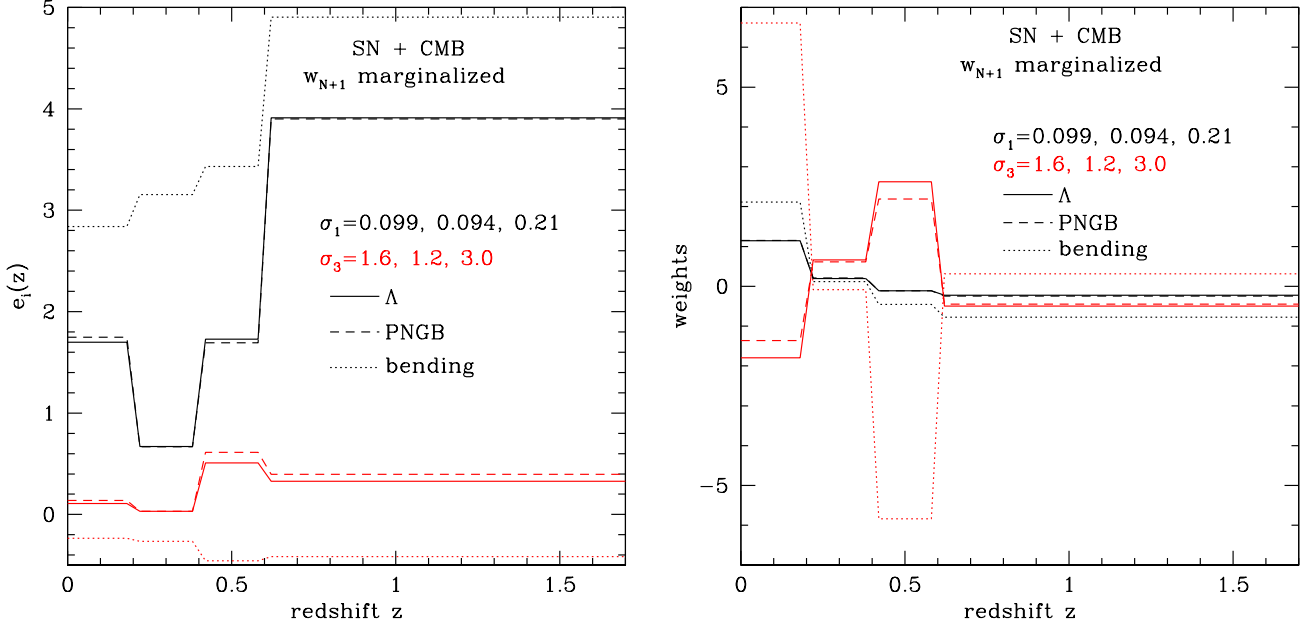


FIG. 14: As Fig. 13, but marginalizing over  $w_{N+1}$ .

where  $\delta p_{n+1} = p_{\text{fix},n+1} - p_{t,n+1}$ , we can use Eq. (25),

$$\delta p_i \equiv p_{e,i} - p_{t,i} = (F^{(n)})_{ij}^{-1} \sum_k \frac{\partial O_k}{\partial p_j} \frac{1}{\sigma_k^2} \Delta O_k, \quad (\text{C2})$$

where the superscript  $(n)$  means that we need the  $n \times n$  Fisher matrix calculated using the first  $n$  parameters (the ones that we have not fixed). Inserting Eq. (C1) into Eq. (C2) gives

$$\delta p_i = -\delta p_{n+1} \times \sum_{j=1}^n (F^{(n)})_{ij}^{-1} (F^{(n+1)})_{j,n+1} \quad (\text{C3})$$

( $i = 1, \dots, n$ ), where we have used Eq. (1) to substitute the  $(n+1) \times (n+1)$  Fisher matrix. We then obtain Eq. (26),

$$\frac{dp_i}{dp_{n+1}} = - \sum_{j=1}^n (F^{(n)})_{ij}^{-1} (F^{(n+1)})_{j,n+1}. \quad (\text{C4})$$

Note that since Eq. (25) is only valid to first order, we can calculate the Fisher matrix using the true parameter values.

- 
- [1] D. Huterer and G. Starkman, Phys.Rev.Lett. **90**, 031301 (2003), arXiv:astro-ph/0207517.
  - [2] R. G. Crittenden and L. Pogosian, arXiv:astro-ph/0510293.
  - [3] C. Shapiro and M. S. Turner, Astrophys.J. **649**, 563 (2006), arXiv:astro-ph/0512586.
  - [4] F. Simpson and S. Bridle, Phys.Rev.D **73**, 083001 (2006), arXiv:astro-ph/0602213.
  - [5] J. Dick, L. Knox, and M. Chu, JCAP **7**, 1 (2006), arXiv:astro-ph/0603247.
  - [6] C. Stephan-Otto, Phys.Rev.D **74**, 023507 (2006), arXiv:astro-ph/0605403.
  - [7] D. Huterer and H. V. Peiris, Phys.Rev.D **75**, 083503 (2007), arXiv:astro-ph/0610427.
  - [8] A. G. Kim, E. V. Linder, R. Miquel, and N. Mostek, MNRAS **347**, 909 (2004), arXiv:astro-ph/0304509.
  - [9] A. J. S. Hamilton and M. Tegmark, MNRAS **312**, 285 (2000), arXiv:astro-ph/9905192.
  - [10] W. Hu and T. Okamoto, Phys.Rev.D **69**, 043004 (2004), arXiv:astro-ph/0308049.

- [11] S. Leach, MNRAS **372**, 646 (2006), arXiv:astro-ph/0506390.
- [12] K. Kadota, S. Dodelson, W. Hu, and E. D. Stewart, Phys.Rev.D **72**, 023510 (2005), arXiv:astro-ph/0505158.
- [13] M. J. Mortonson and W. Hu, arXiv:0705.1132.
- [14] D. Huterer and A. Cooray, Phys.Rev.D **71**, 023506 (2005), arXiv:astro-ph/0404062.
- [15] A. G. Riess *et al.*, Astrophys.J. **659**, 98 (2007), arXiv:astro-ph/0611572.
- [16] S. Sullivan, A. Cooray, and D. E. Holz, JCAP **9**, 4 (2007), arXiv:0706.3730.
- [17] G. Efstathiou and J. R. Bond, MNRAS **304**, 75 (1999), arXiv:astro-ph/9807103.
- [18] E. V. Linder and D. Huterer, Phys.Rev.D **72**, 043509 (2005), arXiv:astro-ph/0505330.
- [19] N. Suzuki, Astrophys.J.Supp. **163**, 110 (2006).
- [20] T. M. Davis, J. B. James, B. P. Schmidt, and A. G. Kim, AIP Conf. Ser. **924**, 330 (2007), arXiv:astro-ph/0701904.
- [21] <http://rkb.home.cern.ch/rkb/AN16pp/node40.html>.
- [22] D. Huterer and M. S. Turner, Phys.Rev.D **64**, 123527 (2001), arXiv:astro-ph/0012510.
- [23] A. Albrecht and G. Bernstein, Phys.Rev.D **75**, 103003 (2007), arXiv:astro-ph/0608269.
- [24] E. V. Linder, Astropart.Phys. **26**, 102 (2006), arXiv:astro-ph/0604280.
- [25] E. V. Linder, arXiv:0708.0024.
- [26] J. A. Frieman, C. T. Hill, A. Stebbins, and I. Waga, Phys.Rev.Lett. **75**, 2077 (1995), arXiv:astro-ph/9505060.
- [27] C. Wetterich, Phys.Lett.B **594**, 17 (2004), arXiv:astro-ph/0403289.
- [28] <http://cosmology.lbl.gov/BOSS>.
- [29] R. R. Caldwell, in Sources and Detection of Dark Matter in the Universe (DM2000), ed. D. Cline, p. 74 (Springer: 2001); [http://www.dartmouth.edu/~caldwell/index\\_files/DM2000.ps](http://www.dartmouth.edu/~caldwell/index_files/DM2000.ps).
- [30] E. V. Linder, Phys.Rev.D **73**, 063010 (2006), arXiv:astro-ph/0601052.
- [31] C.-P. Ma, R. R. Caldwell, P. Bode, and L. Wang, Astrophys.J.Lett. **521**, L1 (1999), arXiv:astro-ph/9906174.
- [32] R. Kallosh, A. Linde, S. Prokushkin, and M. Shmakova, Phys.Rev.D **66**, 123503 (2002), arXiv:hep-th/0208156.
- [33] R. R. Caldwell and E. V. Linder, Phys.Rev.Lett. **95**, 141301 (2005), arXiv:astro-ph/0505494.
- [34] A. Abrahamse, M. Barnard, B. Bozek, and M. Yashar, in preparation.
- [35] E. V. Linder, Phys.Rev.Lett. **90**, 091301 (2003), arXiv:astro-ph/0208512.